Melnikov-type method and homoclinic bifurcation in a class of hybrid piecewise smooth systems under noise and impulsive excitation

Yuxi Li[a], Zhouchao Wei[a,b,c*], Irene Moroz[d]

[a] *School of Mathematics and Physics, China University of Geosciences, Wuhan, 430074, China*

[b] *Institute for Advanced Marine Research, China University of Geosciences, Guangzhou 511462, China*

[c] *Shenzhen Research Institute, China University of Geosciences, Shenzhen, 518000, China*

[d] *Mathematical Institute, University of Oxford, Oxford OX2 6GG, England*

Abstract

In this paper, we developed the classical Melnikov method in a class of general hybrid abstract piecewise smooth systems subjected to elastic and rigid impact effects under noise and impulsive excitation. The relevant unperturbed Hamiltonian systems possess the homoclinic orbit and tristable characteristic. The homoclinic orbit will continuously cross the first two switching manifolds, jump across the third one subjected to the impulsive excitation, then jump about the x-axis on the fourth and last one symmetrically due to the rigid impact effect, but won't cross the last one in the existence of the corresponding unilateral rigid constraint. Specifically, the perturbed trajectories will jump across the first switching manifold by the reset mapping rule about the elastic impact effect. Moreover, our new random Melnikov-type process and function will be got, the criteria of homoclinic chaos about the systems without or with noise excitation can also be obtained. Finally, the homoclinic bifurcation and chaos about a concrete hybrid seven-piecewise feedback control system under saturation and dead zone constrains are analysed and verified through our extended Melnikov-type method and numerical simulations.

Keywords: Random non-smooth Melnikov method, Hybrid piecewise smooth system, Homoclinic bifurcation and chaos, Noise and impulsive excitation

1 Introduction

Piecewise smooth systems [1], as a kind of typical non-smooth dynamical systems, are often used to describe most engineering and natural problems in the real world, such as mechanical systems with impact and collision [2], controlled systems [3, 4], etc [5, 6]. The researches in these parts not only continuously arouse the research interest of more scholars, but also gradually and systematically improve our understanding about non-smooth dynamical systems [7, 8]. Among them, the hot and noteworthy topic is the progressions for chaotic dynamics and global bifurcation in piecewise smooth systems. For the researches of these such same problems about smooth systems [9, 10], the classical Melnikov method [11–13] is regarded as an extremely effective tool [14–16], it also has high dimensional relevant cases [17, 18]. In view of these, further developing the classical

*Corresponding author. E-mail: weizhouchao@163.com

Melnikov method of smooth systems is natural and indispensable [19, 20]. In recent years, the relevant concepts and theories of non-smooth Melnikov method have increasingly rich and systematic than before. Furthermore, the developed non-smooth Melnikov method has also become the most powerful and effective tool to investigate the piecewise smooth systems. However, with the authenticity of the system modelling and the disparities of understanding for global bifurcation in non-smooth dynamical systems, it is extremely urgent to try to extend the relevant results for existing Melnikov method to non-smooth systems influenced by more complex factors to solve the corresponding practical problems.

The phased breakthroughs have been achieved in extending the effective Melnikov analytical theory from smooth to non-smooth systems. In 2000, Kunze [21] firstly gave the discontinuous Melnikov theoretical form in the planar systems. Du et al. [22] analysed several pendulum systems with the actual rigid impact under the help of different non-smooth Melnikov method about different sections separately. The results about homoclinic Melnikov method of Battelli and Fečkan [24] were optimized by Li et al. [23], making the forms of these theoretical results easier to calculate. Granados et al. [25] considered the two-dimensional piecewise smooth subharmonic orbits and the corresponding improved Melnikov analytical theory. Then, Li et al. [26, 27] obtained two kind of piecewise-smooth Melnikov methods about the homoclinic and heteroclinic chaos by combining mapping rules of impact based on [25]. Moreover, Tian et al. [28–30] studied different heteroclinic and homoclinic chaos in several impulsive non-smooth systems through calculating corresponding Melnikov functions in different forms. Zhou et al. [31] considered subharmonic chaos and bifurcation in the vibration isolation systems containing two pairs of oblique springs through the appropriate non-smooth Melnikov theory. Li et al. [32] proposed a theoretical framework and carries out numerical verification for suppressing homoclinic chaos of a class of vibro-impact oscillators by adding non-harmonic periodic excitations based on the non-smooth Melnikov method. Peng et al [33] analysed homoclinic bifurcation for a class of conveyor belt systems with dry friction and impact by deriving the piecewise homoclinic Melnikov function related to the speed of the conveyor belt, then, they investigated homoclinic bifurcation and chaos in a class of SD oscillators under external quasi-periodic excitation with two frequencies by using the non-smooth Melnikov method [34]. Actually, it's of inevitability to describe and consider random excitation corresponding to the randomness in reality when studying relevant bifurcation and chaotic dynamics [35, 36]. Correspondingly, under the influence of random excitation, the mean-square criteria [37, 38] corresponding to the random Melnikov processes and functions in the statistical significance are commonly analysed and utilize [39–41]. Lu [42] investigated the persistence for homoclinic orbits in several second order ordinary differential equations with small white noise by Melnikov-type theory and invariant manifold analysis. Recently, based on the Melnikov analytical results in [43], we [44, 45] theoretically derived the different homoclinic and heteroclinic Melnikov analytical method in piecewise smooth systems containing impulses and noises, then they applied these extended Melnikov-type methods to a concrete vibro-impact mechanical system in [46].

On the other hand, for the application of methods and specific analysis in actual dynamic systems, piecewise linear systems included in piecewise smooth systems are also often regarded to be the very appropriate approximation of most practical non-smooth mechanical systems. For the smooth and discontinuous (SD) oscillator pioneered in [47], Cao et al. [48] confirmed their piecewise linear approximation can effectively study the smooth and discontinuous dynamics of this SD oscillator and even deterministic bistable systems. Han et al. [49] proposed and analysed bifurcations and chaotic dynamics in the limit case for a coupled SD oscillator rigidly composed of two SD oscillators. Zhou et al. [50] employed the corresponding Melnikov method and this kind of

approximation technique to show the global dynamics in the tristable system under the influences of damping and harmonic excitation. Huang et al. [51] proposed a novel spring-rods-mass system with smooth and discontinuous dynamics as well as quasi-zero-stiffness property, then studied chaotic thresholds of this system under the elastic impact by Melnikov method. Zhang et al. [52] analysed the global dynamics for impacting cantilever beam supported by oblique springs through the piecewise approximation method and the non-smooth Melnikov method. In addition, it is common and natural to encounter the multi-piecewise system when modeling the feedback control system under relay, hysteresis, saturation and dead zone constrains. Significantly, Ji et al. [3] investigated the chaos for a simple smooth linear system under a five-piecewise feedback control with saturation and dead zone constrains numerically. On this basis, Li et al. [53] constructed and analysed a corresponding five-piecewise linear feedback control system about saturation and dead zone constrains under periodic excitation and viscous damping by the extended Melnikov method.

Our this work plans to theoretically extend the classical Melnikov method in a class of general hybrid piecewise smooth systems subjected to elastic and rigid impacts under noise and impulsive excitation. Then, the extended Melnikov-type method can be obtained. Moreover, according to [3,53], in view of the hybrid piecewise linear system subjected to elastic impact, rigid impact, noise, impulsive excitation, damping and periodic perturbations, we will give a concrete hybrid seven-piecewise dimensionless systems under feedback control subjected to dead zone and saturation constrains. For the verification of the correctness and effectiveness about our extended method, it will be used to analyse the homoclinic chaotic dynamics in this concrete seven-piecewise system. Here are some highlights of this work. (i): our general systems include the reset mapping rule about the elastic impact, four switching manifolds and random noise, while the system analysed in [28] doesn't have these three influencing factors. (ii): compared with the system studied in our previous paper [44], the general systems we investigated in our this work consider the influence of two additional factors, i.e., unilateral constraints described and induced through rigid impacts, four switching manifolds. (iii): our Melnikov-type function is not same as the functions in [28,44]. However, the corresponding form in which we obtain the results can be reduced or transformed to theirs if simplifying or adjusting our system's some factors. (iv): our given hybrid seven-piecewise system, i.e., an application example of verifying the correctness and effectiveness, is constructed on the basis of a hybrid piecewise linear system, while the system constructed and studied in [3,53] is based on a simple smooth linear system. Therefore, the theoretical part and application in our this work are the extension of [3, 28, 44, 53].

This work's structure is shown below. The new Melnikov theoretical analysis in our investigated systems is described and given, the relevant Melnikov-type process and function are got in section 2, the conditions of homoclinic chaos in the systems without or with noise excitation are obtained by calculating. In section 3, in view of a hybrid piecewise linear system under elastic impact, rigid impact, noise, impulsive excitation, damping and periodic perturbations, a concrete hybrid seven-piecewise system under feedback control subjected to saturation and dead zone constrains is given. Then, the new theoretical results obtained, i.e., the new Melnikov-type method we extended, and relevant numerical simulations are utilized in analysing the given systems. Lastly, section 4 gives our conclusions.

2 Theoretical framework of Melnikov mathematical analysis

2.1 Description of the general hybrid piecewise smooth system

We divide $\mathbb{R}^2$ into five following zones by four Σ_i, then, $\mathbb{R}^2 = S_1 \cup \Sigma_1 \cup S_2 \cup \Sigma_2 \cup S_3 \cup \Sigma_3 \cup S_4 \cup \Sigma_4 \cup S_5$, where

$$\begin{aligned} &S_1 = \left\{(x,y) \in \mathbb{R}^2 \mid x < \alpha_1\right\}, S_2 = \left\{(x,y) \in \mathbb{R}^2 \mid \alpha_1 < x < \alpha_2\right\}, \\ &S_3 = \left\{(x,y) \in \mathbb{R}^2 \mid \alpha_2 < x < \alpha_3\right\}, \ S_4 = \left\{(x,y) \in \mathbb{R}^2 \mid \alpha_3 < x < \alpha_4\right\}, \\ &S_5 = \left\{(x,y) \in \mathbb{R}^2 \mid \alpha_4 < x\right\}, \ \Sigma_1 = \left\{(x,y) \in \mathbb{R}^2 \mid x = \alpha_1\right\}, \\ &\Sigma_2 = \left\{(x,y) \in \mathbb{R}^2 \mid x = \alpha_2\right\}, \ \Sigma_3 = \left\{(x,y) \in \mathbb{R}^2 \mid x = \alpha_3\right\}, \\ &\Sigma_4 = \left\{(x,y) \in \mathbb{R}^2 \mid x = \alpha_4\right\}. \end{aligned} \tag{2.1}$$

and α_i are constants, $\Sigma_i = \Sigma_i^+ \cup \Sigma_i^- \cup \{0\}$, $(i = 1, 2, 3, 4)$.

The following general abstract hybrid piecewise smooth systems subjected to elastic and rigid impact effects under noise and impulsive excitation will be considered in $\mathbb{R}^2$:

$$\begin{cases} \begin{pmatrix} \dot{x} \\ \dot{y} \end{pmatrix} = JDH(x,y) + \varepsilon G(x,y,t) \\ \qquad\qquad = \begin{cases} JDH_1(x,y) + \varepsilon G_1(x,y,t), \ (x,y) \in S_1, \\ JDH_2(x,y) + \varepsilon G_2(x,y,t), \ (x,y) \in S_2, \\ JDH_3(x,y) + \varepsilon G_3(x,y,t), \ (x,y) \in S_3, \\ JDH_4(x,y) + \varepsilon G_4(x,y,t), \ (x,y) \in S_4 \end{cases} \\ \Delta x \mid_{x=\alpha_1,\alpha_2,\alpha_3} = 0, \ \Delta y \mid_{x=\alpha_2} = 0, \ \Delta y \mid_{x=\alpha_1} \neq 0, \\ y^- \mid_{x=\alpha_3} = \gamma_0(1-\varepsilon\eta_2) y^+ \mid_{x=\alpha_3}, \\ y^+ \mid_{x=\alpha_4} = -(1-\varepsilon\eta_1) y^- \mid_{x=\alpha_4}, \end{cases} \tag{2.2}$$

where $0 < \varepsilon \ll 1$, $(x,y) \in \mathbb{R}^2$, four Hamiltonian functions $H_i : \mathbb{R}^2 \to \mathbb{R}$, $G_i(x,y,t) = f_i(x,y,t) + g_i(x,y)\xi(t)$, $f_i : \mathbb{R}^2 \times \mathbb{R} \to \mathbb{R}^2$, $g_i : \mathbb{R}^2 \to \mathbb{R}$. $JDH_i(x,y) = \begin{pmatrix} y \\ h_i(x) \end{pmatrix}$, $f_i(x,y,t) = \begin{pmatrix} 0 \\ f_{i1}(x,y,t) \end{pmatrix}$, $g_i(x,y) = \begin{pmatrix} 0 \\ g_{i1}(x,y) \end{pmatrix}$. A normal vector of different Σ_i can be written as $\mathbf{n} = (1,0)$.
And $x^\pm \mid_{x=\alpha_1,\alpha_2,\alpha_3}$ or $y^\pm \mid_{x=\alpha_1,\alpha_2,\alpha_3}$ represent different right and left limits at x or y,

$$\Delta x \mid_{x=\alpha_1,\alpha_2,\alpha_3} = x^+ \mid_{x=\alpha_1,\alpha_2,\alpha_3} - x^- \mid_{x=\alpha_1,\alpha_2,\alpha_3} .$$

Then, the trajectories of system cross the switching manifold Σ_2 continuously. The reset mapping rule about the elastic impact on Σ_1 is as follows, i.e., the direction of motion remains unchanged,

$$\begin{aligned} \eta_0 : &\Sigma_1 \times \mathbb{R} \to \Sigma_1 \\ &(\alpha_1, y, \varepsilon) \mapsto (\alpha_1, y_\varepsilon) = (\alpha_1, \eta_{0,\varepsilon}(y)), \end{aligned} \tag{2.3}$$

which has $y \cdot \eta_{0,\varepsilon}(y) > 0$ when $y \neq 0$, $\eta_{0,0}(y) = y$, η_0^{-1} represents a inverse map for η_0.
For Σ_3 and Σ_4, we have

$$\begin{aligned} y^- \mid_{x=\alpha_3} &= \gamma_0(1-\varepsilon\eta_2) y^+ \mid_{x=\alpha_3}, \\ y^+ \mid_{x=\alpha_4} &= -(1-\varepsilon\eta_1) y^- \mid_{x=\alpha_4}, \end{aligned} \tag{2.4}$$

where $\gamma_0(1-\varepsilon\eta_2)$ and γ_0 are the change for the perturbed system and unperturbed system on Σ_3 subjected to the impulsive excitation. $y^-\mid_{x=\alpha_4}$ and $y^+\mid_{x=\alpha_4}$ represent the sudden change in y from $y^-\mid_{x=\alpha_4}$ to $y^+\mid_{x=\alpha_4}$ when the rigid impact occurs before and after. $-(1-\varepsilon\eta_1)$ and -1 are the change for perturbed and unperturbed system on Σ_4 due to the presence of unilateral constraint expressed through the rigid impact effect, the direction changes and is reverse. $\gamma_0,\ \eta_1$ and η_2 are three positive parameters $(0<\eta_1,\ \eta_2<1)$. Letting $\Pi_x(x,y)=x$.

As to the corresponding representation of $\xi(t)$, the following Gaussian white noise excitation will be introduced,

$$E\xi(t)=0,\ E\xi(t)\xi(t+\tau)=\begin{cases}\infty\ (\tau=0),\\ 0\ (\tau\neq 0),\end{cases}$$

$S_\xi(\omega_1)$ is the constant spectral density with ω_1. Based on [38, 54], the white noise in the specific derivation process of subsequent random non-smooth Melnikov processes and functions are approximated through the sum for many harmonic functions with some different random phases and frequencies.

According to the detailed explanation in the meanings represented by each part of the above system (2.2)-(2.3), $x=\alpha_i\ (i=1,2,3,4)$ make $\mathbb{R}^2=S_1\cup\Sigma_1\cup S_2\cup\Sigma_2\cup S_3\cup\Sigma_3\cup S_4\cup\Sigma_4\cup S_5$, and the system only corresponds to these four zones $S_i\ (i=1,2,3,4)$ due to the presence for unilateral rigid constraint on Σ_4. The trajectories cross Σ_1 at (x,y), then the reset mapping rule about the elastic impact (2.3) on Σ_1 is used immediately. As to Σ_2, the trajectories continuously cross it. For Σ_3, the trajectory is subjected to impulsive excitation which makes the trajectory jump across Σ_3. For Σ_4, the trajectories jump about x-axis on Σ_4, y instantaneously changes from $(\alpha_4, y^-\mid_{x=\alpha_4})$ to $(\alpha_4, y^+\mid_{x=\alpha_4})$ due to the existence of the rigid impact. And the trajectories won't cross Σ_4 and enter Σ_5 in the presence of the unilateral rigid constraint.

The following assumptions about the orbits and trajectories of system (2.2)-(2.3) shown in Fig. 1 are given,

$\mathbf{L}_1$: For $\forall(\alpha_j,y)\in\Sigma_j$, $[\mathbf{n}\cdot JDH_j(\alpha_j,y)]\cdot[\mathbf{n}\cdot JDH_{j+1}(\alpha_j,y)]>0\ (j=1,2,3)$.

$\mathbf{L}_2$: System (2.2)-(2.3) with $\varepsilon=0$ possess an equilibrium point $p_0=(x_0,y_0)\in S_1$, the piecewise homoclinic orbit $\gamma(t)$ which is symmetric about the axis of x is

$$\gamma(t)=\begin{cases}\gamma_1(t)\in S_1=\begin{cases}\gamma_1^+(t),\ t\le t_1^-,\\ \gamma_1^-(t),\ t\ge t_7^+,\end{cases}\\ \gamma_2(t)\in S_2=\begin{cases}\gamma_2^+(t),\ t_1^+\le t\le t_2^-,\\ \gamma_2^-(t),\ t_6^+\le t\le t_7^-,\end{cases}\\ \gamma_3(t)\in S_3=\begin{cases}\gamma_3^+(t),\ t_2^+\le t\le t_3^-,\\ \gamma_3^-(t),\ t_5^+\le t\le t_6^-,\end{cases}\\ \gamma_4(t)\in S_4=\begin{cases}\gamma_4^+(t),\ t_3^+\le t\le t_4^-,\\ \gamma_4^-(t),\ t_4^+\le t\le t_5^-,\end{cases}\end{cases}\tag{2.5}$$

where $t_k^\pm\ (k=1,\cdots,7)$ correspond to the time when the above homoclinic orbit reaches and leaves

Σ_i $(i = 1, 2, 3, 4)$.

$$
\begin{aligned}
\gamma_1^+(t_1^-) &= [x_1^+(t_1^-), y_1^+(t_1^-)]^T = (\alpha_1, y_1)^T, \\
\gamma_2^+(t_1^+) &= [x_2^+(t_1^+), y_2^+(t_1^+)]^T = (\alpha_1, y_1)^T, \\
\gamma_2^+(t_2^-) &= [x_2^+(t_2^-), y_2^+(t_2^-)]^T = (\alpha_2, y_2)^T, \\
\gamma_3^+(t_2^+) &= [x_3^+(t_2^+), y_3^+(t_2^+)]^T = (\alpha_2, y_2)^T, \\
\gamma_3^+(t_3^-) &= [x_3^+(t_3^-), y_3^+(t_3^-)]^T = (\alpha_3, y_2)^T, \\
\gamma_3^+(t_3^+) &= [x_3^+(t_3^+), y_3^+(t_3^+)]^T = (\alpha_3, y_3)^T, \\
\gamma_4^+(t_4^-) &= [x_4^+(t_4^-), y_4^+(t_4^-)]^T = (\alpha_4, y_4)^T,
\end{aligned}
\tag{2.6}
$$

and the expressions for $\gamma_4^-(t_4^+)$, $\gamma_4^-(t_5^-)$, $\gamma_3^-(t_5^+)$, $\gamma_3^-(t_6^-)$, $\gamma_2^-(t_6^+)$, $\gamma_2^-(t_7^-)$, $\gamma_1^-(t_7^+)$ are similar to (2.6).

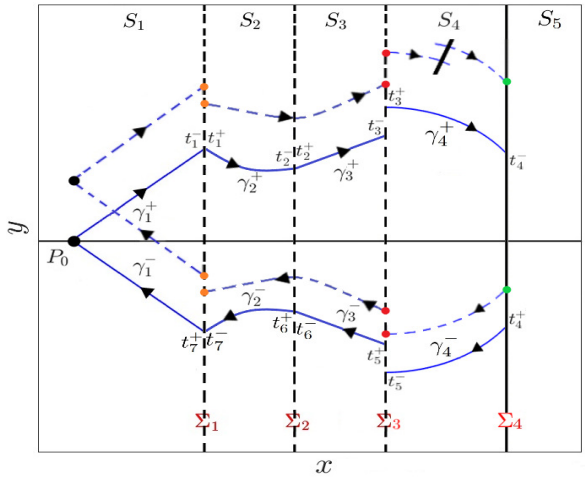


Fig. 1. The homoclinic connection in system (2.2)-(2.3) for $\varepsilon = 0$(Blue solid line), the unstable and stable manifolds of perturbed homoclinic orbit in system (2.2)-(2.3)(Blue dotted line).

2.2 Main results of the Melnikov-type function and method

In this subsection, we will give the derivation process for our new Melnikov-type function and method about system (2.2)-(2.3). In the following Melnikov-type random process and mathematical analysis [11, 12], the stable and unstable manifolds about the perturbed systems presented below and shown in Fig. 1 will be broken and intersect within S_4.

The perturbed orbit [43–45] $q^{u(s)}(t, t_0, \varepsilon), (0 < \varepsilon \ll 1)$ are

$$
q^u(t, t_0, \varepsilon) = \begin{cases}
q^{u,1}(t, t_0, \varepsilon) = \gamma_1^+(t - t_0) + \varepsilon q_1^{u,1}(t, t_0) + O(\varepsilon^2), \ t \le t_{1,\varepsilon}^-, \\
q^{u,2}(t, t_0, \varepsilon) = \gamma_2^+(t - t_0) + \varepsilon q_1^{u,2}(t, t_0) + O(\varepsilon^2), \ t_{1,\varepsilon}^+ \le t \le t_{2,\varepsilon}^-, \\
q^{u,3}(t, t_0, \varepsilon) = \gamma_3^+(t - t_0) + \varepsilon q_1^{u,3}(t, t_0) + O(\varepsilon^2), \ t_{2,\varepsilon}^+ \le t \le t_{3,\varepsilon}^-, \\
q^{u,4}(t, t_0, \varepsilon) = \gamma_4^+(t - t_0) + \varepsilon q_1^{u,4}(t, t_0) + O(\varepsilon^2), \ t_{3,\varepsilon}^+ \le t \le t_0
\end{cases}
\tag{2.7}
$$

$$q^s(t,t_0,\varepsilon)=\begin{cases} q^{s,5}(t,t_0,\varepsilon)=\gamma_4^+(t-t_0)+\varepsilon q_1^{s,5}(t,t_0)+O(\varepsilon^2),\ t_0\le t\le t_{4,\varepsilon}^-,\\ q^{s,4}(t,t_0,\varepsilon)=\gamma_4^-(t-t_0)+\varepsilon q_1^{s,4}(t,t_0)+O(\varepsilon^2),\ t_{4,\varepsilon}^+\le t\le t_{5,\varepsilon}^-,\\ q^{s,3}(t,t_0,\varepsilon)=\gamma_3^-(t-t_0)+\varepsilon q_1^{s,3}(t,t_0)+O(\varepsilon^2),\ t_{5,\varepsilon}^+\le t\le t_{6,\varepsilon}^-,\\ q^{s,2}(t,t_0,\varepsilon)=\gamma_2^-(t-t_0)+\varepsilon q_1^{s,2}(t,t_0)+O(\varepsilon^2),\ t_{6,\varepsilon}^+\le t\le t_{7,\varepsilon}^-,\\ q^{s,1}(t,t_0,\varepsilon)=\gamma_1^-(t-t_0)+\varepsilon q_1^{s,1}(t,t_0)+O(\varepsilon^2),\ t\ge t_{7,\varepsilon}^+, \end{cases} \tag{2.8}$$

where $t_{k,\varepsilon}^{\pm}$ $(k=1,\cdots,7)$ correspond to the point of time when $q^{u(s)}(t,t_0,\varepsilon)$ leave and reach Σ_1, Σ_2, Σ_3, Σ_4, $t_{k,\varepsilon}^-=t_{k,\varepsilon}^+$,

$$t_{k,\varepsilon}^{\pm}=t_k^{\pm}+t_0+\varepsilon t_{k,1}^{\pm}+O(\varepsilon^2), \tag{2.9}$$

$$\begin{aligned} &q^{u(s),i}(t,t_0,\varepsilon)=[x^{u(s),i}(t,t_0,\varepsilon),\ y^{u(s),i}(t,t_0,\varepsilon)]^T,\ (i=1,2,3,4),\\ &q^{s,5}(t,t_0,\varepsilon)=[x^{s,5}(t,t_0,\varepsilon),\ y^{s,5}(t,t_0,\varepsilon)]^T, \end{aligned} \tag{2.10}$$

$$\begin{aligned} &q^{u,1}(t_{1,\varepsilon}^-,t_0,\varepsilon)\neq q^{u,2}(t_{1,\varepsilon}^+,t_0,\varepsilon),\ q^{s,1}(t_{7,\varepsilon}^+,t_0,\varepsilon)\neq q^{s,2}(t_{7,\varepsilon}^-,t_0,\varepsilon),\\ &q^{u,2}(t_{2,\varepsilon}^-,t_0,\varepsilon)=q^{u,3}(t_{2,\varepsilon}^+,t_0,\varepsilon),\ q^{s,2}(t_{6,\varepsilon}^+,t_0,\varepsilon)=q^{s,3}(t_{6,\varepsilon}^-,t_0,\varepsilon),\\ &q^{u,3}(t_{3,\varepsilon}^-,t_0,\varepsilon)\neq q^{u,4}(t_{4,\varepsilon}^+,t_0,\varepsilon),\ q^{s,3}(t_{5,\varepsilon}^+,t_0,\varepsilon)\neq q^{s,4}(t_{5,\varepsilon}^-,t_0,\varepsilon),\\ &q^{s,4}(t_{4,\varepsilon}^+,t_0,\varepsilon)\neq q^{s,5}(t_{4,\varepsilon}^-,t_0,\varepsilon). \end{aligned} \tag{2.11}$$

And $q_1^{u(s),i}(t,t_0)$ $(i=1,2,3,4)$ and $q_1^{s,4}(t,t_0)$ are governed by

$$\begin{aligned} &\dot q_1^{u(s),i}(t,t_0)=JD^2H_i(\gamma(t-t_0))\cdot q_1^{u(s),i}(t,t_0)+G_i(\gamma(t-t_0),t),\\ &\dot q_1^{s,5}(t,t_0)=JD^2H_4(\gamma(t-t_0))\cdot q_1^{s,5}(t,t_0)+G_4(\gamma(t-t_0),t). \end{aligned} \tag{2.12}$$

Letting

$$\begin{aligned} &\triangle_\varepsilon^{u(s),i}(t,t_0)=\varepsilon JDH_i(\gamma(t-t_0))\wedge q_1^{u(s),i}(t,t_0),\\ &\triangle_\varepsilon^{s,5}(t,t_0)=\varepsilon JDH_4(\gamma(t-t_0))\wedge q_1^{s,5}(t,t_0). \end{aligned} \tag{2.13}$$

Differentiating (2.13) with (2.12), we obtain

$$\begin{aligned} &\dot\triangle_\varepsilon^{u(s),i}(t,t_0)=\varepsilon JDH_i(\gamma(t-t_0))\wedge G_i(\gamma(t-t_0),t),\\ &\dot\triangle_\varepsilon^{s,5}(t,t_0)=\varepsilon JDH_4(\gamma(t-t_0))\wedge G_4(\gamma(t-t_0),t) \end{aligned} \tag{2.14}$$

where $i=1,2,3,4$, $\triangle_\varepsilon^{u,1}(-\infty,t_0)=\triangle_\varepsilon^{s,1}(+\infty,t_0)=0$ due to $JDH_1(p_0)=0$, and $q_1^{u(s),i}(t,t_0)$ are bounded.

Then, measuring the distance between $q^u(t_0,t_0,\varepsilon)$ and $q^s(t_0,t_0,\varepsilon)$, we have

$$\begin{aligned}
\triangle_\varepsilon(t_0) =& \triangle_\varepsilon^{u,4}(t_0,t_0) - \triangle_\varepsilon^{s,5}(t_0,t_0) + O(\varepsilon^2)\\
=&[\triangle_\varepsilon^{u,4}(t_0,t_0) - \triangle_\varepsilon^{u,4}(t_0+t_3^+,t_0)] + [\triangle_\varepsilon^{u,4}(t_0+t_3^+,t_0) - \triangle_\varepsilon^{u,3}(t_0+t_3^-,t_0)]\\
&+ [\triangle_\varepsilon^{u,3}(t_0+t_3^-,t_0) - \triangle_\varepsilon^{u,3}(t_0+t_2^+,t_0)] + [\triangle_\varepsilon^{u,3}(t_0+t_2^+,t_0) - \triangle_\varepsilon^{u,3}(t_0+t_2^-,t_0)]\\
&+ [\triangle_\varepsilon^{u,2}(t_0+t_2^-,t_0) - \triangle_\varepsilon^{u,2}(t_0+t_1^+,t_0)] + [\triangle_\varepsilon^{u,2}(t_0+t_1^+,t_0) - \triangle_\varepsilon^{u,1}(t_0+t_1^-,t_0)]\\
&+ [\triangle_\varepsilon^{u,1}(t_0+t_1^-,t_0) - \triangle_\varepsilon^{u,1}(-\infty,t_0)] + [\triangle_\varepsilon^{u,1}(-\infty,t_0) - \triangle_\varepsilon^{s,1}(+\infty,t_0)]\\
&+ [\triangle_\varepsilon^{s,1}(+\infty,t_0) - \triangle_\varepsilon^{s,1}(t_0+t_7^+,t_0)] + [\triangle_\varepsilon^{s,1}(t_0+t_7^+,t_0) - \triangle_\varepsilon^{s,2}(t_0+t_7^-,t_0)]\\
&+ [\triangle_\varepsilon^{s,2}(t_0+t_7^-,t_0) - \triangle_\varepsilon^{s,2}(t_0+t_6^+,t_0)] + [\triangle_\varepsilon^{s,2}(t_0+t_6^+,t_0) - \triangle_\varepsilon^{s,3}(t_0+t_6^-,t_0)]\\
&+ [\triangle_\varepsilon^{s,3}(t_0+t_6^-,t_0) - \triangle_\varepsilon^{s,3}(t_0+t_5^+,t_0)] + [\triangle_\varepsilon^{s,3}(t_0+t_5^+,t_0) - \triangle_\varepsilon^{s,4}(t_0+t_5^-,t_0)]\\
&+ [\triangle_\varepsilon^{s,4}(t_0+t_5^-,t_0) - \triangle_\varepsilon^{s,4}(t_0+t_4^+,t_0)] + [\triangle_\varepsilon^{s,4}(t_0+t_4^+,t_0) - \triangle_\varepsilon^{s,5}(t_0+t_4^-,t_0)]\\
&+ [\triangle_\varepsilon^{s,5}(t_0+t_4^-,t_0) - \triangle_\varepsilon^{s,5}(t_0,t_0)] + O(\varepsilon^2)\\
=&\varepsilon\int_{-\infty}^{+\infty} JDH(\gamma(t-t_0)) \wedge G(\gamma(t-t_0),t)dt + I_1 + I_2 + [\triangle_\varepsilon^{u,2}(t_0+t_1^+,t_0) - \triangle_\varepsilon^{u,1}(t_0+t_1^-,t_0)]\\
&+ [\triangle_\varepsilon^{s,1}(t_0+t_7^+,t_0) - \triangle_\varepsilon^{s,2}(t_0+t_7^-,t_0)] + O(\varepsilon^2),
\end{aligned} \tag{2.15}$$

where

$$I_1 = [\triangle_\varepsilon^{u,4}(t_0+t_3^+,t_0) - \triangle_\varepsilon^{u,3}(t_0+t_3^-,t_0)] + [\triangle_\varepsilon^{s,3}(t_0+t_5^+,t_0) - \triangle_\varepsilon^{s,4}(t_0+t_5^-,t_0)], \tag{2.16}$$

$$I_2 = [\triangle_\varepsilon^{s,4}(t_0+t_4^+,t_0) - \triangle_\varepsilon^{s,5}(t_0+t_4^-,t_0)], \tag{2.17}$$

$$\begin{aligned}
\triangle_\varepsilon^{u,1}(t_0+t_1^-,t_0) &= \varepsilon\int_{-\infty}^{t_1^-+t_0} JDH_1(\gamma(t-t_0)) \wedge G_1(\gamma(t-t_0),t)dt,\\
-\triangle_\varepsilon^{s,1}(t_0+t_7^+,t_0) &= \varepsilon\int_{t_7^++t_0}^{+\infty} JDH_1(\gamma(t-t_0)) \wedge G_1(\gamma(t-t_0),t)dt.
\end{aligned} \tag{2.18}$$

Firstly, we will calculate $\triangle_\varepsilon^{u,2}(t_0+t_1^+,t_0)$, $\triangle_\varepsilon^{s,2}(t_0+t_7^-,t_0)$. Then, **Theorem 2.1** will be given.

Theorem 2.1.

$$\triangle_\varepsilon^{u,2}(t_0+t_1^+,t_0) = \varepsilon\dot\gamma_2^+(t_1^+) \wedge \frac{\partial\eta_0(\gamma(t_1^-),0)}{\partial\varepsilon} + \frac{\boldsymbol{n}(\gamma(t_1^-))\cdot D^*\eta_0(\gamma(t_1^-),0)\dot\gamma_2^+(t_1^+)}{\boldsymbol{n}(\gamma(t_1^-))\cdot\dot\gamma_1^+(t_1^-)} \times \triangle_\varepsilon^{u,1}(t_0+t_1^-,t_0), \tag{2.19}$$

$$\triangle_\varepsilon^{s,2}(t_0+t_7^-,t_0) = \varepsilon\dot\gamma_2^-(t_7^-) \wedge \frac{\partial\eta_0^{-1}(\gamma(t_7^+),0)}{\partial\varepsilon} + \frac{\boldsymbol{n}(\gamma(t_7^+))\cdot D^*\eta_0^{-1}(\gamma(t_7^+),0)\dot\gamma_2^-(t_7^-)}{\boldsymbol{n}(\gamma(t_7^+))\cdot\dot\gamma_1^-(t_7^+)} \times \triangle_\varepsilon^{s,1}(t_0+t_7^+,t_0), \tag{2.20}$$

where

$$D\eta_0(\gamma(t_1^-),0) = \begin{pmatrix} 0 & 0 \\ \frac{\partial\eta_{0,0}}{\partial y}(\Pi_y\gamma(t_1^-)) \end{pmatrix},\ D\eta_0^{-1}(\gamma(t_7^+),0) = \begin{pmatrix} 0 & 0 \\ \frac{\partial\eta_{0,0}^{-1}}{\partial y}(\Pi_y\gamma(t_7^+)) \end{pmatrix},$$

and $D^*\eta_0(\gamma(t_1^-),0)$, $D^*\eta_0^{-1}(\gamma(t_7^+),0)$ *represent adjoint corresponding to* $D\eta_0(\gamma(t_1^-),0)$, $D\eta_0^{-1}(\gamma(t_7^+),0)$.

Proof. For $t \in (t_{1,\varepsilon}^+, t_{2,\varepsilon}^-)$, a equation below is written,

$$q^{u,2}(t,t_0,\varepsilon) = \eta_0(q^{u,1}(t_{1,\varepsilon}^-,t_0,\varepsilon),\varepsilon) + \int_{t_{1,\varepsilon}^+}^t JDH_2(q^{u,2}(s,t_0,\varepsilon)) + \varepsilon G_2(q^{u,2}(s,t_0,\varepsilon))ds. \tag{2.21}$$

Then, we differentiate (2.21) with ε, substitute $t_1^+ + t_0$ into t and 0 into ε,

$$\begin{aligned} q_1^{u,2}(t_0+t_1^+,t_0) =& \frac{\partial \eta_0(\gamma(t_1^-),0)}{\partial \varepsilon} + D\eta_0(\gamma(t_1^-),0) q_1^{u,1}(t_0+t_1^-,t_0) \\ &+ [D\eta_0(\gamma(t_1^-),0)\dot{\gamma}_1^+(t_1^-) - \dot{\gamma}_2^+(t_1^+)] \frac{dt_{1,\varepsilon}^+}{d\varepsilon}|_{\varepsilon=0}. \end{aligned} \tag{2.22}$$

With regard to $q^{u,1}(t_{1,\varepsilon}^-, t_0, \varepsilon) \in \Sigma_1$, the following equation can be obtained

$$\Pi_x(q^{u,1}(t_{1,\varepsilon}^-, t_0, \varepsilon)) = \alpha_1. \tag{2.23}$$

Next, we also differentiate (2.23) with ε, let $\varepsilon = 0$, due to $t_{1,\varepsilon}^+ = t_{1,\varepsilon}^-$, there is

$$\frac{dt_{1,\varepsilon}^+}{d\varepsilon}|_{\varepsilon=0} = -\frac{\mathbf{n}(\gamma(t_1^-)) \cdot q_1^{u,1}(t_0+t_1^-,t_0)}{\mathbf{n}(\gamma(t_1^-)) \cdot \dot{\gamma}_1^+(t_1^-)} \tag{2.24}$$

Thus, we substitute (2.24) and (2.22) into (2.13), the above equation in (2.19) can be derived,

$$\begin{aligned} \triangle_\varepsilon^{u,2}(t_0+t_1^+,t_0) =& \varepsilon JDH_2(\gamma(t_1^+)) \wedge q_1^{u,2}(t_0+t_1^+,t_0) \\ =& \varepsilon\dot{\gamma}_2^+(t_1^+) \wedge \left\{ \frac{\partial \eta_0(\gamma(t_1^-),0)}{\partial \varepsilon} + \big[D\eta_0(\gamma(t_1^-),0) \right. \\ &+ \left. \frac{[\dot{\gamma}_2^+(t_1^+) - D\eta_0(\gamma(t_1^-),0)\dot{\gamma}_1^+(t_1^-)]\mathbf{n}(\gamma(t_1^-))}{\mathbf{n}(\gamma(t_1^-)) \cdot \dot{\gamma}_1^+(t_1^-)} \right] q_1^{u,1}(t_0+t_1^-,t_0) \Big\} \\ =& \varepsilon\dot{\gamma}_2^+(t_1^+) \wedge \frac{\partial \eta_0(\gamma(t_1^-),0)}{\partial \varepsilon} + \varepsilon \frac{\mathbf{n}(\gamma(t_1^-)) \cdot D^*\eta_0(\gamma(t_1^-),0)\dot{\gamma}_2^+(t_1^+)}{\mathbf{n}(\gamma(t_1^-)) \cdot \dot{\gamma}_1^+(t_1^-)} \\ &\times \dot{\gamma}_1^+(t_1^-) \wedge q_1^{u,1}(t_0+t_1^-,t_0) \\ =& \varepsilon\dot{\gamma}_2^+(t_1^+) \wedge \frac{\partial \eta_0(\gamma(t_1^-),0)}{\partial \varepsilon} + \frac{\mathbf{n}(\gamma(t_1^-)) \cdot D^*\eta_0(\gamma(t_1^-),0)\dot{\gamma}_2^+(t_1^+)}{\mathbf{n}(\gamma(t_1^-)) \cdot \dot{\gamma}_1^+(t_1^-)} \times \triangle_\varepsilon^{u,1}(t_0+t_1^-,t_0). \end{aligned} \tag{2.25}$$

The proof for (2.20) is the same as (2.19), thus, omitting here. □

Secondly, I_1 and I_2 are calculated.

Let

$$\begin{aligned} &\triangle_1^{u(s),i}(t,t_0) = JDH_i(\gamma(t-t_0)) \wedge q^{u(s),i}(t,t_0), \\ &\triangle_1^{s,5}(t,t_0) = JDH_4(\gamma(t-t_0)) \wedge q^{s,5}(t,t_0). \end{aligned} \tag{2.26}$$

According to [28,29], we know

$$\begin{aligned} I_1 + I_2 =& [\triangle_\varepsilon^{u,4}(t_0+t_3^+,t_0) - \triangle_\varepsilon^{u,3}(t_0+t_3^-,t_0)] + [\triangle_\varepsilon^{s,3}(t_0+t_5^+,t_0) - \triangle_\varepsilon^{s,4}(t_0+t_5^-,t_0)] \\ &+ [\triangle_\varepsilon^{s,4}(t_0+t_4^+,t_0) - \triangle_\varepsilon^{s,5}(t_0+t_4^-,t_0)] \\ =& [\triangle_1^{u,4}(t_0+t_3^+,t_0) - \triangle_1^{u,3}(t_0+t_3^-,t_0)] + [\triangle_1^{s,3}(t_0+t_5^+,t_0) - \triangle_1^{s,4}(t_0+t_5^-,t_0)] \\ &+ [\triangle_1^{s,4}(t_0+t_4^+,t_0) - \triangle_1^{s,5}(t_0+t_4^-,t_0)] \end{aligned} \tag{2.27}$$

From [29], we know that $q^{u,4}(t_{3,\varepsilon}^+, t_0, \varepsilon)$ can become

$$q^{u,4}(t_{3,\varepsilon}^+, t_0, \varepsilon) = q^{u,4}(t_3^+ + t_0, t_0, \varepsilon) + \varepsilon t_{3,1}^+ JDH_4(q^{u,4}(t_3^+ + t_0, t_0, \varepsilon)), \tag{2.28}$$

Based on (2.7), (2.8) and (2.28), there are

$$t_{3,1}^+ = -\frac{x_4^{u,4}(t_3^+ + t_0, t_0)}{y_4^+(t_3^+)} + O(\varepsilon), \tag{2.29}$$

$$y^{u,4}(t^+_{3,\varepsilon},t_0,\varepsilon)=y^+_4(t^+_3)+\varepsilon t^+_{3,1}h_4(x^+_4(t^+_3))+\varepsilon y^{u,4}_1(t^+_3+t_0,t_0)+O(\varepsilon^2), \tag{2.30}$$

similarly,

$$t^-_{5,1}=-\frac{x^{s,4}_4(t^-_5+t_0,t_0)}{y^-_4(t^-_5)}+O(\varepsilon), \tag{2.31}$$

$$y^{s,4}(t^-_{5,\varepsilon},t_0,\varepsilon)=y^-_4(t^-_5)+\varepsilon t^-_{5,1}h_4(x^-_4(t^-_5))+\varepsilon y^{s,4}_1(t^-_5+t_0,t_0)+O(\varepsilon^2), \tag{2.32}$$

$$t^+_{4,1}=-\frac{x^{s,4}_4(t^+_4+t_0,t_0)}{y^-_4(t^+_4)}+O(\varepsilon), \tag{2.33}$$

$$y^{s,5}(t^-_{4,\varepsilon},t_0,\varepsilon)=y^+_4(t^-_4)+\varepsilon t^-_{4,1}h_4(x^+_4(t^-_4))+\varepsilon y^{s,5}_1(t^-_4+t_0,t_0)+O(\varepsilon^2). \tag{2.34}$$

Substituting (2.28) into (2.26), we get

$$\begin{aligned}I_1+I_2=&[y^+_4(t^+_3)y^{u,4}(t^+_{3,\varepsilon},t_0,\varepsilon)-y^+_3(t^-_3)y^{u,3}(t^-_{3,\varepsilon},t_0,\varepsilon)]\\&+[y^-_3(t^+_5)y^{s,3}(t^+_{5,\varepsilon},t_0,\varepsilon)-y^-_4(t^-_5)y^{s,4}(t^-_{5,\varepsilon},t_0,\varepsilon)]\\&+[y^-_4(t^+_4)y^{s,4}(t^+_{4,\varepsilon},t_0,\varepsilon)-y^+_4(t^-_4)y^{s,5}(t^-_{4,\varepsilon},t_0,\varepsilon)].\end{aligned} \tag{2.35}$$

And from (2.4), we get

$$\begin{aligned}y^+_4(t^+_3)&=\frac{1}{\gamma_0}y^+_3(t^-_3),\\y^{u,4}(t^+_{3,\varepsilon},t_0,\varepsilon)&=\frac{(1-\varepsilon\eta_2)}{\gamma_0}y^{u,3}(t^-_{3,\varepsilon},t_0,\varepsilon),\\y^-_3(t^+_5)&=\gamma_0y^-_4(t^-_5),\\y^{s,3}(t^+_{5,\varepsilon},t_0,\varepsilon)&=(1-\varepsilon\eta_2)\gamma_0y^{s,4}(t^-_{5,\varepsilon},t_0,\varepsilon),\\y^-_4(t^+_4)&=-y^+_4(t^-_4),\\y^{s,4}(t^+_{4,\varepsilon},t_0,\varepsilon)&=-(1-\varepsilon\eta_1)y^{s,5}(t^-_{4,\varepsilon},t_0,\varepsilon).\end{aligned} \tag{2.36}$$

Thus,

$$\begin{aligned}I_1+I_2=&[1-(1+\varepsilon\eta_2)\gamma_0^2]y^+_4(t^+_3)y^{u,4}(t^+_{3,\varepsilon},t_0,\varepsilon)\\&+[(1-\varepsilon\eta_2)\gamma_0^2-1]y^-_4(t^-_5)y^{s,4}(t^-_{5,\varepsilon},t_0,\varepsilon)-\varepsilon\eta_1y^+_4(t^-_4)y^{s,5}(t^-_{4,\varepsilon},t_0,\varepsilon)\\=&\varepsilon[-2\eta_2[y^+_3(t^-_3)]^2+(\gamma_0^2-1)[[y^-_4(t^-_5)y^{s,4}_1(t^-_5+t_0,t_0)-x^{s,4}_1(t^-_5+t_0,t_0)h_4(x^-_4(t^-_5))]\\&-[y^+_4(t^+_3)y^{u,4}_1(t^+_3+t_0,t_0)-x^{u,4}_1(t^+_3+t_0,t_0)h_4(x^+_4(t^+_3))]]-\eta_1[y^+_4(t^-_4)]^2]+O(\varepsilon^2)\\=&\varepsilon[-2\eta_2[y^+_3(t^-_3)]^2+(\gamma_0^2-1)\left(\int^{t^-_5+t_0}_{t^+_4+t_0}JDH_4(\gamma^-_4(t-t_0))\wedge G_4(\gamma^-_4(t-t_0),t)dt+\right.\\&\left.\int^{t^-_4+t_0}_{t^+_3+t_0}JDH_4(\gamma^+_4(t-t_0))\wedge G_4(\gamma^+_4(t-t_0),t)dt\right)-\eta_1[y^+_4(t^-_4)]^2]+O(\varepsilon^2).\end{aligned} \tag{2.37}$$

According to [29], there are

$$\begin{aligned}[y^+_3(t^-_3)]^2=&2\int^{\alpha_1}_{x_0}h_1(x)dx+2\int^{\alpha_2}_{\alpha_1}h_2(x)dx+2\int^{\alpha_3}_{\alpha_2}h_3(x)dx\\[y^+_4(t^-_4)]^2=&\frac{2}{\gamma_0^2}\int^{\alpha_1}_{x_0}h_1(x)dx+\frac{2}{\gamma_0^2}\int^{\alpha_2}_{\alpha_1}h_2(x)dx+\frac{2}{\gamma_0^2}\int^{\alpha_3}_{\alpha_2}h_3(x)dx+2\int^{\alpha_4}_{\alpha_3}h_4(x)dx.\end{aligned} \tag{2.38}$$

Then, substituting (2.18), (2.19), (2.20), (2.37), (2.38) into (2.15), we can derive the following specific random non-smooth Melnikov-type function,

$$M(t_0)=M_d(t_0)+M_r(t_0), \tag{2.39}$$

where

$$
\begin{aligned}
M_d(t_0) =&\dot{\gamma}_2^+(t_1^+) \wedge \frac{\partial \eta_0(\gamma(t_1^-),0)}{\partial \varepsilon} - \dot{\gamma}_2^-(t_7^-) \wedge \frac{\partial \eta_0^{-1}(\gamma(t_7^+),0)}{\partial \varepsilon} \\
&+ \frac{\mathbf{n}(\gamma(t_1^-)) \cdot D^* \eta_0(\gamma(t_1^-),0)\dot{\gamma}_2^+(t_1^+)}{\mathbf{n}(\gamma(t_1^-)) \cdot \dot{\gamma}_1^+(t_1^-)} \times \int_{-\infty}^{t_1^-} JDH_1(\gamma_1^+(t)) \wedge f_1(\gamma_1^+(t), t+t_0)dt \\
&+ \int_{t_1^+}^{t_2^-} JDH_2(\gamma_2^+(t)) \wedge f_2(\gamma_2^+(t), t+t_0)dt + \int_{t_6^+}^{t_7^-} JDH_2(\gamma_2^-(t)) \wedge f_2(\gamma_2^-(t), t+t_0)dt \\
&+ \int_{t_2^+}^{t_3^-} JDH_3(\gamma_3^+(t)) \wedge f_3(\gamma_3^+(t), t+t_0)dt + \int_{t_5^+}^{t_6^-} JDH_3(\gamma_3^-(t)) \wedge f_3(\gamma_3^-(t), t+t_0)dt \\
&+ \gamma_0^2 \left(\int_{t_3^+}^{t_4^-} JDH_4(\gamma_4^+(t)) \wedge f_4(\gamma_4^+(t), t+t_0)dt + \int_{t_4^+}^{t_5^-} JDH_4(\gamma_4^-(t)) \wedge f_4(\gamma_4^+(t), t+t_0)dt \right) \\
&- 4\eta_2 \left(\int_{x_0}^{\alpha_1} h_1(x)dx + \int_{\alpha_1}^{\alpha_2} h_2(x)dx + \int_{\alpha_2}^{\alpha_3} h_3(x)dx \right) \\
&- 2\eta_1 \left(\frac{1}{\gamma_0^2} \int_{x_0}^{\alpha_1} h_1(x)dx + \frac{1}{\gamma_0^2} \int_{\alpha_1}^{\alpha_2} h_2(x)dx + \frac{1}{\gamma_0^2} \int_{\alpha_2}^{\alpha_3} h_3(x)dx + \int_{\alpha_3}^{\alpha_4} h_4(x)dx \right) \\
&+ \frac{\mathbf{n}(\gamma(t_7^+)) \cdot D^* \eta_0^{-1}(\gamma(t_7^+),0)\dot{\gamma}_2^-(t_7^-)}{\mathbf{n}(\gamma(t_7^+)) \cdot \dot{\gamma}_1^-(t_7^+)} \times \int_{t_7^+}^{+\infty} JDH_1(\gamma_1^-(t)) \wedge f_1(\gamma_1^-(t), t+t_0)dt,
\end{aligned}
\tag{2.40}
$$

and

$$
\begin{aligned}
M_r(t_0) =&\frac{\mathbf{n}(\gamma(t_1^-)) \cdot D^* \eta_0(\gamma(t_1^-),0)\dot{\gamma}_2^+(t_1^+)}{\mathbf{n}(\gamma(t_1^-)) \cdot \dot{\gamma}_1^+(t_1^-)} \times \int_{-\infty}^{t_1^-} JDH_1(\gamma_1^+(t)) \wedge g_1(\gamma_1^+(t))\xi(t+t_0)dt \\
&+ \int_{t_1^+}^{t_2^-} JDH_2(\gamma_2^+(t)) \wedge g_2(\gamma_2^+(t))\xi(t+t_0)dt + \int_{t_6^+}^{t_7^-} JDH_2(\gamma_2^-(t)) \wedge g_2(\gamma_2^-(t))\xi(t+t_0)dtdt \\
&+ \int_{t_2^+}^{t_3^-} JDH_3(\gamma_3^+(t)) \wedge g_3(\gamma_3^+(t))\xi(t+t_0)dt + \int_{t_5^+}^{t_6^-} JDH_3(\gamma_3^-(t)) \wedge g_3(\gamma_3^-(t))\xi(t+t_0)dt \\
&+ \gamma_0^2 \left(\int_{t_3^+}^{t_4^-} JDH_4(\gamma_4^+(t)) \wedge g_4(\gamma_4^+(t))\xi(t+t_0)dt + \int_{t_4^+}^{t_5^-} JDH_4(\gamma_4^-(t)) \wedge g_4(\gamma_4^-(t))\xi(t+t_0)dt \right) \\
&+ \frac{\mathbf{n}(\gamma(t_7^+)) \cdot D^* \eta_0^{-1}(\gamma(t_7^+),0)\dot{\gamma}_2^-(t_7^-)}{\mathbf{n}(\gamma(t_7^+)) \cdot \dot{\gamma}_1^-(t_7^+)} \times \int_{t_7^+}^{+\infty} JDH_1(\gamma_1^-(t)) \wedge g_1(\gamma_1^-(t))\xi(t+t_0)dt.
\end{aligned}
\tag{2.41}
$$

We treat the random part of $M(t_0)$ in the statistical sense [43], and $M_r(t_0)$ with convolution form is

$$
M_r(t_0) = l(t) * \xi(t), \tag{2.42}
$$

here

$$l(t)=\begin{cases}\dfrac{\mathbf{n}(\gamma(t_1^-))\cdot D^*\eta_0(\gamma(t_1^-),0)\dot{\gamma}_2^+(t_1^+)}{\mathbf{n}(\gamma(t_1^-))\cdot\dot{\gamma}_1^+(t_1^-)}\times\left[JDH_1(\gamma_1^+(t))\wedge g_1(\gamma_1^+(t))\right],\ t\le t_1^-,\\ JDH_2(\gamma_2^+(t))\wedge g_2(\gamma_2^+(t)),\ t_1^+\le t\le t_2^-,\\ JDH_3(\gamma_3^+(t))\wedge g_3(\gamma_3^+(t)),\ t_2^+\le t\le t_3^-,\\ \gamma_0^2[JDH_4(\gamma_4^+(t))\wedge g_4(\gamma_4^+(t))],\ t_3^+\le t\le t_4^-,\\ \gamma_0^2[JDH_4(\gamma_4^-(t))\wedge g_4(\gamma_4^-(t))],\ t_4^+\le t\le t_5^-,\\ JDH_3(\gamma_3^-(t))\wedge g_3(\gamma_3^-(t)),\ t_5^+\le t\le t_6^-,\\ JDH_2(\gamma_2^-(t))\wedge g_2(\gamma_2^-(t)),\ t_6^+\le t\le t_7^-,\\ \dfrac{\mathbf{n}(\gamma(t_7^+))\cdot D^*\eta_0^{-1}(\gamma(t_7^+),0)\dot{\gamma}_2^-(t_7^-)}{\mathbf{n}(\gamma(t_7^+))\cdot\dot{\gamma}_1^-(t_7^+)}\times[JDH_1(\gamma_1^-(t))\wedge g_1(\gamma_1^-(t))],\ t\ge t_7^+.\end{cases}\tag{2.43}$$

Then, we regard $l(t)$ and $\xi(t)$ as the impulse response and the system's input, respectively. We have

$$H_0(\omega_1)=\int_{-\infty}^{+\infty}l(t)e^{-j\omega_1 t}dt.\tag{2.44}$$

And

$$E\left[M(t_0)\right]=M_d,\tag{2.45}$$

where the variance of $M_r(t_0)$ is

$$\begin{aligned}\sigma_r^2=&E\left[(M_r(t_0))^2\right]-\left[E\left[M_r(t_0)\right]\right]^2\\ =&\int_{-\infty}^{+\infty}|H_0(\omega_1)|^2S_\xi(\omega_1)d\omega,\end{aligned}\tag{2.46}$$

$M(t_0)$ varies between $M_d-\sigma_r$ and $M_d+\sigma_r$ with standard deviation σ_r.
In view of [12,39,43,44], the above Melnikov-type mathematical derivation process and (2.39), the following **Theorem 2.2** will be derived.

Theorem 2.2. *(i) If $M_d(t_0)=0$, $M(t_0)$ has some simple zeros about t_0 under the mean sense. (ii) If $M_d(t_0)\neq 0$, $M(t_0)$ has some simple zeros about t_0 under the mean square sense when $M_d^2(t_0)=\sigma_r^2$.*

Remark 1. If the formula (2.39) possesses the statistical sense simple zero points, the stable and unstable manifold of system (2.2)-(2.3) will be intersected transversally. Then, from [11,12], this class of systems will occur homoclinic bifurcation and exist chaos. Additionally, $M_d(t_0)=0$ is the homoclinic chaos criteria under Smale horseshoes sense of system (2.2)-(2.3) when noise excitation doesn't exist. Then, the extended Melnikov-type method of the homoclinic bifurcation and chaos is derived.

Remark 2. Next, on the one hand, we will provide the overall elaboration and discussion to the practical significance of the Melnikov theoretical framework proposed in Section 2. Taking engineering systems with feedback control and chaotic oscillations in mechanical systems as examples, we will discuss the extension and application of Melnikov method within this theoretical framework to non-smooth systems in various real-world scenarios.

In many real-world engineering systems, especially in the fields of automatic control and signal processing, feedback control is crucial. Engineering systems with feedback control may encounter various non-smooth factors in practical operation, such as amplitude limiting, relay switching, etc. The key points, steps, and methods used in the theoretical extension and application of the Melnikov process in other real-world non-smooth engineering systems with feedback control are similar

to those in our this study. The reason is that this study applies the extended random non-smooth Melnikov result to a concrete hybrid seven-piecewise system under feedback control. However, some differences are that other real-world non-smooth engineering systems are more complex, subject to more external environmental influences, and more susceptible to the coupling effects of various random non-smooth factors. Significantly, real-world engineering systems generally have high-dimensional characteristics. At this point, it is necessary to comprehensively introduce new dimensionality reduction and decoupling methods, as well as new energy-time scale transformations, based on the high-dimensional, random, and non-smooth characteristics contained in the studied system. These will result in a new dimensionality reduction form of the system in the energy coordinate. Then, referring to the theoretical framework Section 2 of our this study, we will derive the corresponding new Melnikov function and summarize the new Melnikov theoretical method. For the practical significance of the application for this extended new Melnikov theoretical method, it can analyze the orbital deviation and stability changes of the real-world engineering systems before and after introducing feedback control from a global perspective, and reveal physical phenomena such as period doubling, the generation of chaotic attractors, etc. Through the deep understanding of systems' behavior within this Melnikov framework, feedback control strategies can be optimized to help identify key parameter ranges and system sensitivities, and predict possible failure modes of the engineering systems under feedback control, thereby ensuring safe and stable operation of the system in engineering applications.

In mechanical systems, especially non-smooth systems involving impact and friction, such as pendulum impact systems, vibration impact systems, vibrating screens, etc., chaotic oscillations often occur. This oscillation will affect the actual stability and performance of the system. For the application research of the Melnikov process in the chaotic oscillation of actual non-smooth mechanical systems, the key points, steps, and methods are similar to our elaboration in the relevant issues of engineering systems with feedback control mentioned above. For its practical application, the extended Melnikov method can help us gain a deeper understanding of the dynamic behavior for mechanical systems, reveal the mechanism of chaotic oscillation, and provide important reference for systems' optimization design and control. Specifically, this extended Melnikov method can reveal the vibration characteristics and laws of the system under different parameter conditions, especially under the influence of noise excitation, external disturbances, and other practical situations, by analyzing the sudden changes, phase trajectory shifts, and behaviors near non-smooth critical points that occur during the global transition process of this system. For example, when structures such as bridges and buildings are affected by earthquakes or wind, complex dynamic responses may occur. This extended Melnikov theoretical method can identify the conditions that cause resonance or instability, providing a basis for designing seismic or wind resistant devices and reducing the risk of system failure due to chaotic oscillations.

Remark 3. On the other hand, the significance and importance of noise excitation, damping, impulsive excitation and other physical phenomena of the system studied within this framework will also be elaborated in detail.

In many practical systems, noise excitation is inevitable, especially in scenarios where external environmental perturbations or internal system oscillations occur. When introducing noise excitation factors, the orbital stability and chaotic behavior of the system will be significantly affected, and in the extension process of the corresponding Melnikov method, it is also necessary to additionally combine random response methods to handle the corresponding noise terms. By extending the Melnikov method to analyze the impact of noise on orbital bifurcations and trajectory offsets, it is helpful to predict the behavior changes of the system in noisy environments and understand

the random response behavior of the system, thereby guiding the control and optimization of the system in practical applications. These also have guiding significance for many other application scenarios, such as evaluating the impact of signal noise on stability in communication systems, or analyzing the impact of random perturbations on market volatility in financial markets.

Damping is the mechanism of energy dissipation, which can affect the vibration characteristics and stability of the system. In practical engineering systems such as mechanical oscillations, damping can reduce the amplitude of chaotic oscillations or guide the system to restore the stable state. By introducing damping into the analytical framework of the extended Melnikov method, the behavior of actual systems can be more accurately described. The resulting extended method helps to understand the behavioral changes of systems from chaotic oscillation states to stable states, especially, those controlled by damping, such as shock absorbers, vehicle suspension systems, etc. The damping term in non-smooth systems not only helps predict energy decay, but also analyzes its suppression effect on orbital deviation. These can help extend the Melnikov method in a wider range of systems, and corresponding extensions can better estimate the damping effect of structures under extreme conditions, thereby improving the anti-interference ability and safety of the system.

Impulsive excitation is a sudden excitation in a system, which is related to the environment in which the system is located or sudden changes within the system. It can cause sudden changes in the evolution and dynamic behavior of the system. Impulsive excitation can cause system vibration and generate impact effects within the system. These will cause resonance phenomenon, gradually increase the amplitude of the system, and pose a threat to the system structure. Considering the dynamics and evolution of the system under impulsive excitation in the framework of extending the Melnikov theoretical method can help us reveal the instantaneous mutation characteristics and dynamic response of the system, which provides the basis for understanding the robustness of the system and the design of corresponding control strategies.

Remark 4. If $\eta_0(\alpha_1, y, \varepsilon) = (\alpha_1, y)$, $g_i = 0$ $(i = 1, 2, 3, 4)$, $t_1^+ = t_2^-$, $t_6^+ = t_7^-$, i.e., Σ_2 doesn't exist, system (2.2)-(2.3) are able to become the general piecewise smooth system under impulse, the rigid impact, two switching manifolds and three zones, then our $M(t_0)$ in (2.39) will be reduced to the form obtained in [28].

Remark 5. If $t_1^+ = t_2^-$, $t_6^+ = t_7^-$, i.e., Σ_2 and the unilateral rigid constraint Σ_4 don't exist, system (2.2)-(2.3) will become the system studied in our previous paper [44]. Then, our $M(t_0)$ in (2.39) will be reduced to the form obtained in [44].

Thus, we have mainly developed the theoretical part of [28,44] from the theoretical perspective. Next, the above Melnikov-type method we extended will be applied in analysing a concrete hybrid seven-piecewise feedback control system to verify the correctness and effectiveness of this method.

3 Application example and numerical simulations

3.1 Application to a concrete hybrid seven-piecewise feedback control system

According to [3, 53], based on the plant whose motion is governed by a single-degree-of-freedom (SDOF) hybrid piecewise system with elastic impact, rigid impact, noise excitation, impulsive excitation, damping and periodic perturbations, we consider a concrete hybrid seven-piecewise

system under feedback control in the following form, as shown in Fig. 2.

$$\begin{cases} \ddot{x} + 2\mu\dot{x} + x + F(x) = f_0\cos(\omega t) + \delta\xi(t), & x < 1, \\ \ddot{x} + 2\mu\dot{x} - x + F(x) = f_0\cos(\omega t) + \delta\xi(t), & 1 \le x < \dfrac{3}{2}, \\ \ddot{x} + 2\mu\dot{x} + x - \dfrac{3}{2} + F(x) = f_0\cos(\omega t) + \delta\xi(t), & \dfrac{3}{2} < x < 2, \\ \eta_0 : (\alpha_1, \dot{x}, \varepsilon) \mapsto (\alpha_1, \eta_{0,\varepsilon}(\dot{x})), \\ \dot{x}^- \mid_{x=\frac{3}{2}} = \gamma_0(1-\varepsilon\eta_2)\dot{x}^+ \mid_{x=\frac{3}{2}}, \\ \dot{x}^+ \mid_{x=2} = -(1-\varepsilon\eta_1)\dot{x}^- \mid_{x=2}, \end{cases} \tag{3.1}$$

where the actuator is subjected to saturation and dead zone constrains. Dead zone caused by the insensitivity of the actual actuator to small inputs means that the output is zero. Saturation caused by the limitation of the actual actuator means that the output reaches saturation value. The motion for controlled system, i.e., the plant, is switched by the dimensionless displacement constraint about x. ω and f_0 are the frequency and coefficient for periodic excitation, μ denotes the damping coefficient, δ is the intensity for Gaussian white noise excitation $\xi(t)$. The fourth equation in (3.1) is the reset mapping rule about the elastic impact of the plant motion. The fifth and sixth equations in (3.1) represent the change of the plant motion subjected to the impulsive excitation and the rigid impact described by unilateral constraint. γ_0 is the coefficient of sudden change in speed without energy lost, $\gamma_0(1-\varepsilon\eta_2)$ and $-(1-\varepsilon\eta_1)$ are the coefficients of sudden change in speed with energy loss. The piecewise linear function $F(x)$ about x with parameters $\beta,\ \alpha_1(0 < \beta < \alpha_1 < 1)$ is the dimensionless output of the actuator subjected to saturation and dead zone constrains corresponding to the simple feedback control in Fig. 3, i.e.,

$$F(x) = \begin{cases} 0, & |x| \le \beta, \\ -\dfrac{1}{\alpha_1 - \beta}(x - \beta\mathrm{sign}(x)), & \beta < |x| < \alpha_1, \\ -\mathrm{sign}(x), & x \le -\alpha_1 \text{ and } \alpha_1 < x < 1, \\ 0, & 1 \le x. \end{cases} \tag{3.2}$$

Let $\dot{x} = y,\ \mu = \varepsilon\overline{\mu},\ f_0 = \varepsilon\overline{f},\ \delta = \varepsilon\overline{\delta}$, we denote again $(\overline{\mu},\ \overline{f_0},\ \overline{\delta})$ by $(\mu,\ f_0,\ \delta)$ $(0 < \varepsilon \ll 1)$. Then, the piecewise unperturbed Hamiltonian function corresponding to system (3.1) is

$$H(x,y) = \begin{cases} H_1(x,y) = \frac{1}{2}y^2 + \frac{1}{2}x^2 - \dfrac{\beta^2}{2(1+\beta-\alpha_1)}, & |x| \le \beta, \\ H_2(x,y) = \frac{1}{2}y^2 + \frac{1}{2}x^2 - \dfrac{1}{2(\alpha_1-\beta)}\left(x - \beta\mathrm{sign}(x)\right)^2 - \dfrac{\beta^2}{2(1+\beta-\alpha_1)}, & \beta < |x| < \alpha_1, \\ H_3(x,y) = \frac{1}{2}y^2 + \frac{1}{2}x^2 - x\mathrm{sign}(x) - \dfrac{\alpha_1^2 - \alpha_1 - \beta}{2(1+\beta-\alpha_1)}, & x \le -\alpha_1 \text{ and } \alpha_1 < x < 1, \\ H_4(x,y) = \frac{1}{2}y^2 - \frac{1}{2}x^2 - \dfrac{\alpha_1^2 - \alpha_1 - \beta}{2(1+\beta-\alpha_1)}, & 1 \le x < \dfrac{3}{2}, \\ H_5(x,y) = \frac{1}{2}y^2 + \frac{1}{2}x^2 - \dfrac{3}{2}x, & \dfrac{3}{2} < x < 2. \end{cases} \tag{3.3}$$

Moreover, the five-piecewise linear system studied in [53] is regarded to be a simplified case for the seven-piecewise linear system (3.1) we constructed when the plant changes from a hybrid piecewise linear system to a simple smooth linear system and

$$F(x) = \begin{cases} 0, & |x| \le \beta, \\ -\dfrac{1}{\alpha_1 - \beta}(x - \beta\mathrm{sign}(x)), & \beta < |x| < \alpha_1, \\ -\mathrm{sign}(x), & \alpha_1 \le |x|. \end{cases} \tag{3.4}$$

The piecewise linear system studied in [53] has five equilibria, i.e., $(0,0)$, $\left(\pm\dfrac{\beta}{1+\beta-\alpha_1}\right)$, $(\pm 1,0)$, and the piecewise homoclinic and heteroclinic solutions as shown in Fig. 4(a) when $\beta=\dfrac{3}{10}$, $\alpha_1=\dfrac{4}{5}$. With the same parameter values, system (3.1) has the piecewise homoclinic and heteroclinic solutions as shown in Fig. 4(b). Meanwhile, we only consider the piecewise homoclinic orbit connecting $\left(\dfrac{3}{5},0\right)$ to itself.

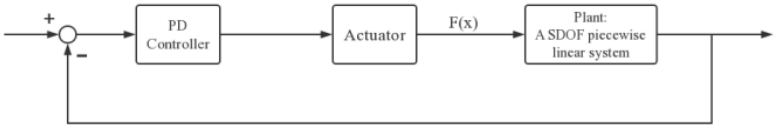


Fig. 2. Block diagram of a class of SDOF hybrid piecewise systems under feedback control where the actuator is subjected to saturation and dead zone constrains.

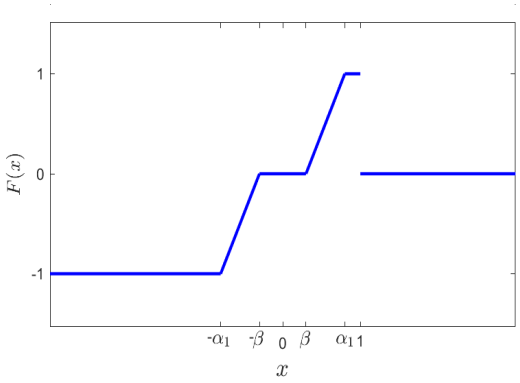


Fig. 3. The piecewise function $F(x)$ corresponding to the output of the actuator subjected to saturation and dead zone constrains.

In this section, the homoclinic bifurcation and chaotic dynamics of the single-degree-of-freedom hybrid piecewise feedback control system subjected to saturation and dead zone constrains with or without noise excitation, i.e., system (3.1), are investigated by our extended Melnikov-type

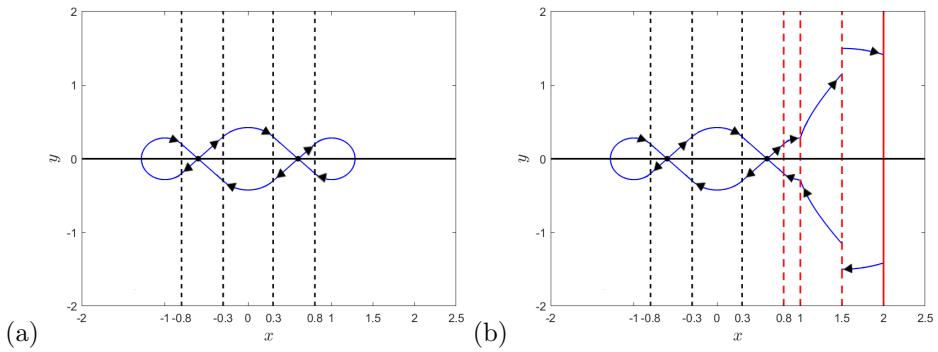


Fig. 4. The piecewise homoclinic and heteroclinic solutions of (a): system studied in [53] for $\varepsilon = 0$ and (b): the hybrid piecewise feedback control system (3.1) we considered for $\varepsilon = 0$.

method. Then, system (3.1)-(3.2) with $\beta = \frac{3}{10}$, $\alpha_1 = \frac{4}{5}$ becomes:

$$\begin{cases} \begin{cases} \dot{x} = y, \\ \dot{y} = -x + \varepsilon\left[-2\mu y + f_0\cos(\omega t) + \delta\xi(t)\right], \end{cases} & |x| \le \frac{3}{10}, \\ \begin{cases} \dot{x} = y, \\ \dot{y} = x - \frac{3}{5}\mathrm{sign}(x) + \varepsilon\left[-2\mu y + f_0\cos(\omega t) + \delta\xi(t)\right], \end{cases} & \frac{3}{10} < |x| < \frac{4}{5}, \\ \begin{cases} \dot{x} = y, \\ \dot{y} = -x + \mathrm{sign}(x) + \varepsilon\left[-2\mu y + f_0\cos(\omega t) + \delta\xi(t)\right], \end{cases} & x \le -\frac{4}{5} \text{ and } \frac{4}{5} < x < 1, \\ \begin{cases} \dot{x} = y, \\ \dot{y} = x + \varepsilon\left[-2\mu y + f_0\cos(\omega t) + \delta\xi(t)\right], \end{cases} & 1 \le x < \frac{3}{2}, \\ \begin{cases} \dot{x} = y, \\ \dot{y} = -x + \frac{3}{2} + \varepsilon\left[-2\mu y + f_0\cos(\omega t) + \delta\xi(t)\right], \end{cases} & \frac{3}{2} < x < 2, \\ \Delta x\,|_{x=\frac{4}{5},1} = 0,\ \Delta y\,|_{x=1} = 0,\ \Delta y\,|_{x=\frac{4}{5}} \neq 0, \\ y^-\,|_{x=\frac{3}{2}} = \frac{\sqrt{133}}{15}(1-\varepsilon\eta_2)y^+\,|_{x=\frac{3}{2}}, \\ y^+\,|_{x=2} = -(1-\varepsilon\eta_1)y^-\,|_{x=2}\,. \end{cases} \tag{3.5}$$

The above reset mapping rule about $x = \frac{4}{5}$ becomes

$$\eta_0 : (\frac{4}{5}, y, \varepsilon) \mapsto (\frac{4}{5}, y_\varepsilon) = \begin{cases} \left(\frac{4}{5}, \frac{y}{1+\varepsilon\rho_0 y}\right), & y > 0, \\ \left(\frac{4}{5}, \frac{y}{1-\varepsilon\rho_0 y}\right), & y < 0, \end{cases} \tag{3.6}$$

where ρ_0 is a positive parameter and

$$\eta_0^{-1} : (\frac{4}{5}, y, \varepsilon) \mapsto (\frac{4}{5}, y_\varepsilon) = \begin{cases} \left(\frac{4}{5}, \frac{y}{1-\varepsilon\rho_0 y}\right), & y > 0, \\ \left(\frac{4}{5}, \frac{y}{1+\varepsilon\rho_0 y}\right), & y < 0. \end{cases} \tag{3.7}$$

Furthermore,

$$H(x,y)=\begin{cases} H_1(x,y)=\frac{1}{2}y^2+\frac{1}{2}x^2-\dfrac{9}{100}, & |x|\le\dfrac{3}{10},\\ H_2(x,y)=\frac{1}{2}y^2+\frac{1}{2}x^2-\left[x-\dfrac{3}{10}\mathrm{sign}(x)\right]^2-\dfrac{9}{100}, & \dfrac{3}{10}<|x|<\dfrac{4}{5},\\ H_3(x,y)=\frac{1}{2}y^2+\frac{1}{2}x^2-x\mathrm{sign}(x)+\dfrac{23}{50}, & x\le-\dfrac{4}{5}\text{ and }\dfrac{4}{5}<x<1,\\ H_4(x,y)=\frac{1}{2}y^2-\frac{1}{2}x^2+\dfrac{23}{50}, & 1\le x<\dfrac{3}{2},\\ H_5(x,y)=\frac{1}{2}y^2+\frac{1}{2}x^2-\dfrac{3}{2}x, & \dfrac{3}{2}<x<2. \end{cases} \tag{3.8}$$

A saddle point $p_0=(x_0,y_0)=\left(\dfrac{3}{5},0\right)$ is one of equilibria of the unperturbed system (3.5)-(3.6). The above piecewise homoclinic orbit about p_0 shown in Fig. 4(b) is written as

$$\gamma(t)=\begin{cases} \left(\dfrac{3}{5}+\dfrac{1}{5}\exp(t+t_a),\dfrac{1}{5}\exp(t+t_a)\right), & t\le t_1^-,\\ \left(1+\dfrac{\sqrt{2}}{5}\cos(t),-\dfrac{\sqrt{2}}{5}\sin(t)\right), & t_1^+\le t\le t_2^-,\\ \left(\dfrac{\sqrt{23}}{5}\sec(-t-t_b),-\dfrac{\sqrt{23}}{5}\tan(-t-t_b)\right), & t_2^+\le t\le t_3^-,\\ \left(\dfrac{3}{2}+\dfrac{3}{2}\cos(t+t_c),\dfrac{3}{2}\sin(t+t_c)\right), & t_3^+\le t\le t_4^-,\\ \left(\dfrac{3}{2}+\dfrac{3}{2}\cos(t-t_d),-\dfrac{3}{2}\sin(t-t_d)\right), & t_4^+\le t\le t_5^-,\\ \left(\dfrac{\sqrt{23}}{5}\sec(t_e-t),\dfrac{\sqrt{23}}{5}\tan(t_e-t)\right), & t_5^+\le t\le t_6^-,\\ \left(1+\dfrac{\sqrt{2}}{5}\cos(t_f-t),\dfrac{\sqrt{2}}{5}\sin(t_f-t)\right), & t_6^+\le t\le t_7^-,\\ \left(\dfrac{3}{5}+\dfrac{1}{5}\exp(t_g-t),-\dfrac{1}{5}\exp(t_g-t)\right), & t\ge t_7^+, \end{cases} \tag{3.9}$$

where $t_a=2.356194$, $t_b=1.857553$, $t_c=2.551328$, $t_d=3.731858$, $t_e=4.425633$, $t_f=9.424779$, $t_g=11.780973$, $t_1^{\pm}=-2.356194$, $t_2^{\pm}=-1.570796$, $t_3^{\pm}=-0.980532$, $t_4^{\pm}=4.962817$, $t_5^{\pm}=5.302654$, $t_6^{\pm}=10.995575$, $t_7^{\pm}=11.780973$. According to (3.6)-(3.9),

$$\begin{aligned} &\gamma_1^+(t_1^-)=\gamma_2^+(t_1^+)=\left(1,\frac{1}{5}\right)=(1,y_1),\\ &\gamma_2^-(t_7^-)=\gamma_1^-(t_7^+)=\left(1,-\frac{1}{5}\right)=(1,-y_1), \end{aligned} \tag{3.10}$$

$$\frac{\partial\eta_0(\gamma(t_1^-),0)}{\partial\varepsilon}=(0,-\rho_0y_1^2),\ \frac{\partial\eta_0^{-1}(\gamma(t_7^+),0)}{\partial\varepsilon}=(0,-\rho_0(-y_1)^2). \tag{3.11}$$

In view of our new Melnikov-type function in (2.39), we can obtained the following formula by substituting and calculating,

$$M(t_0)=-2\rho_0y_1^3-2\mu A+f_0\sqrt{B_1^2+B_2^2}\sin(\omega t_0+\phi)-\frac{133}{50}\eta_2-\frac{450}{133}\eta_1+\int_{-\infty}^{+\infty}l(t)\xi(t+t_0)dt \tag{3.12}$$

where

$$A = 9.910218,\ \tan(\phi) = \frac{B_2}{B_1},$$

$$\begin{aligned}
B_1 = &\int_1^{\frac{3}{2}} \cos\left(\omega\left[-\text{arcsec}\left(\frac{5x}{\sqrt{23}}\right) - t_b\right]\right) - \cos\left(\omega\left[-\text{arcsec}\left(\frac{5x}{\sqrt{23}}\right) + t_e\right]\right) dx \\
&+ \frac{1}{10(\omega^4-1)}\left[4\omega^2\cos(\omega t_1^{\pm}) - 4\omega\sin(\omega t_1^{\pm}) + 2\sqrt{2}\omega(1+\omega^2)\sin(\omega t_2^{\pm}) - 15\omega(1+\omega^2)\sin(\omega t_3^{\pm})\right. \\
&+10(1+\omega^2)(\cos(\omega t_4^{\pm}) + 2\sqrt{2}\omega\sin(\omega t_4^{\pm})) - 15\omega(1+\omega^2)\sin(\omega t_5^{\pm}) + 2\sqrt{2}\omega(1+\omega^2)\sin(\omega t_6^{\pm}) \\
&\left.+4\cos(\omega t_7^{\pm}) - 4\omega\sin(\omega t_7^{\pm})\right], \\
B_2 = &\int_1^{\frac{3}{2}} \sin\left(\omega\left[-\text{arcsec}\left(\frac{5x}{\sqrt{23}}\right) - t_b\right]\right) - \sin\left(\omega\left[-\text{arcsec}\left(\frac{5x}{\sqrt{23}}\right) + t_e\right]\right) dx \\
&+ \frac{1}{10(\omega^4-1)}\left[4\omega\cos(\omega t_1^{\pm}) + 4\omega^2\sin(\omega t_1^{\pm}) - 2\sqrt{2}\omega(1+\omega^2)\cos(\omega t_2^{\pm}) + 15\omega(1+\omega^2)\cos(\omega t_3^{\pm})\right. \\
&-10(1+\omega^2)(2\sqrt{2}\omega\cos(\omega t_4^{\pm}) - \sin(\omega t_4^{\pm})) + 15\omega(1+\omega^2)\cos(\omega t_5^{\pm}) - 2\sqrt{2}\omega(1+\omega^2)\cos(\omega t_6^{\pm}) \\
&\left.+4\omega\cos(\omega t_7^{\pm}) + 4\sin(\omega t_7^{\pm})\right],
\end{aligned}$$

and $l(t)$ is

$$l(t) = \begin{cases}
\frac{\delta}{5}\exp(t+t_a), & t \le t_1^-, \\
-\frac{\sqrt{2}\delta}{5}\sin(t), & t_1^+ \le t \le t_2^-, \\
-\frac{\sqrt{23}\delta}{5}\tan(-t-t_b), & t_2^+ \le t \le t_3^-, \\
\frac{3\gamma_0^2\delta}{2}\sin(t+t_c), & t_3^+ \le t \le t_4^-, \\
-\frac{3\gamma_0^2\delta}{2}\sin(t-t_d), & t_4^+ \le t \le t_5^-, \\
\frac{\sqrt{23}\delta}{5}\tan(t_e-t), & t_5^+ \le t \le t_6^-, \\
\frac{\sqrt{2}\delta}{5}\sin(t_f-t), & t_6^+ \le t \le t_7^-, \\
-\frac{\delta}{5}\exp(t_g-t), & t \ge t_7^+.
\end{cases} \tag{3.13}$$

Then, the following two cases without and with noise excitation can be derived by **Theorem 2.2** and **Remark 1**,

Case A: $\delta = 0$

The noise excitation $\xi(t)$ doesn't exist, $M(t_0)$ has simple zeros with t_0 if

$$|2\rho_0 y_1^3 + 2\mu A + \frac{450}{133}\eta_1 + \frac{133}{50}\eta_2| < f_0\sqrt{B_1^2 + B_2^2}. \tag{3.14}$$

Case B: $\delta \neq 0$

Based on (2.46), there is

$$\sigma_r^2 = \frac{1}{2\pi}\int_{-\infty}^{+\infty}\left[\int_{-\infty}^{+\infty} l(t)\cos(\omega_1 t)dt\right]^2 d\omega_1. \tag{3.15}$$

The noise excitation $\xi(t)$ exists, $M(t_0)$ has simple zeros under the mean-square sense with t_0 if

$$\left(2\rho_0 y_1^3 + 2\mu A + \frac{450}{133}\eta_1 + \frac{133}{50}\eta_2\right)^2 < f_0^2(B_1^2 + B_2^2) + \sigma_r^2. \tag{3.16}$$

3.2 Numerical simulations

These analytical results, the correctness for our new method, the homoclinic bifurcation and chaos in system (3.5)-(3.6) will be tested and verified by the following numerical simulations and the corresponding explanations.

Letting $\varepsilon = 0.01,\ \eta_1 = \eta_2 = 0.1$. The chaos and homoclinic bifurcation thresholds in system (3.5)-(3.6) under $\rho_0 = 0.5,\ \delta = 0$ calculated through (3.14) under $\mu = 0.05,\ 0.2,\ 0.4,\ 0.8$ are described within Fig 5(a). The thresholds about homoclinic chaos in system (3.5)-(3.6) under $\rho_0 = 0.5,\ \delta = 0$ calculated through (3.14) with $\rho_0 = 0.1,\ 0.4,\ 0.7,\ 1$ are described within Fig 5(b). The thresholds about homoclinic chaos for system (3.5)-(3.6) with $\rho_0 = 0.1,\ \omega = 1.75$ calculated through (3.16) under $\mu = 0.01,\ 0.11,\ 0.21,\ 0.31$ described within Fig 6(a). The thresholds about homoclinic chaos in system (3.5)-(3.6) under $\mu = 0.5,\ f_0 = 11.5$ calculated through (3.16) about $\rho_0 = 0.1,\ 0.4,\ 0.7,\ 1$ are described within Fig. 6(b). The surface about the thresholds in system (3.5)-(3.6) about $\rho_0 = 0.5,\ \delta = 0$ in (ω, μ, f_0) space is described within Fig. 7(a). The homoclinic chaotic surface for system (3.5)-(3.6) about $\mu = 0.5,\ \rho_0 = 0.1,\ \eta_1 = 0.1,\ f_0 = 10$ in (ω, η_2, δ) space is described within Fig. 7(b). In view of Fig. 5-Fig. 7, the homoclinic bifurcation and chaos complicated dynamics will occur within the regions above the each critical curve and surface.

As to the homoclinic chaos in system (3.5)-(3.6), the parameters we chose in the following all numerical simulations guarantee that existing the homoclinic orbit with transversality. We take $\mu = 0.6,\ \varepsilon = 0.01,\ \omega = 1.25,\ \eta_1 = 1,\ \eta_2 = 0.1,\ \rho_0 = 0.9$. For the noise excitation $\xi(t)$ doesn't exist with $\delta = 0$, homoclinic chaos states in system (3.5)-(3.6) about $f_0 = 12.6,\ 14,\ 19,\ 22,\ 26.5,\ 34$ are within Fig. 8. The phase portrait and the corresponding time serie in system (3.5)-(3.6) under $\delta = 0$ and $f_0 = 41$ are shown within Fig. 9 to better demonstrate the state of system's chaos. For the noise excitation $\xi(t)$ exists, homoclinic chaotic dynamics in system (3.5)-(3.6) under the corresponding parameter $f_0 = 14,\ \delta = 0.000001,\ 0.7,\ 3.5,\ 6$ are shown within Fig. 11(a)-Fig. 11(d). When δ increases from small to big within the small range, the degree for chaotic state in system (3.5)-(3.6) will deepen as shown in Fig. 11. However, the chaotic degree will weaken as shown within Fig. 11(c) to Fig. 11(d) if δ go on increasing within the big range. The representative phenomena of chaotic dissipation in the system (3.5)-(3.6) has also been weakened. These results and representative phenomena demonstrate that the transformation of noise excitation intensity δ can suppress and enhance chaotic degree in system (3.5)-(3.6). From the comparison results between Fig. 11(a) and Fig. 8(b), it can be seen that even introducing extremely low intensity in noise $\delta = 0.000001$ will also have the significant effects about chaotic state and phase portraits in system (3.5)-(3.6) under the same periodic excitation $f_0 = 14$. Subsequently, the 0-1 test method for chaos [55,56] will be used to further test and show those above results of system (3.5)-(3.6). If the test value of correlation coefficient K_c is close to 0, i.e., $K_c \approx 0$, then the system's new trajectories within the newly established coordinates are bounded and the corresponding dynamical behaviours of system (3.5)-(3.6) are regular. Conversely, if the test value is close to 1, i.e., $K_c \approx 1$, then the system's new trajectories within the newly established coordinates are unbounded, i.e., Brownian-like, and the corresponding dynamical behaviours of system (3.5)-(3.6) are chaotic. Afterwards, for the noise excitation $\xi(t)$ doesn't exist with $\delta = 0$, we will first apply this kind of test method to system (3.5)-(3.6), the system's new trajectories and phase portraits within the newly established coordinates $p(n)$ and $q(n)$ under $f_0 = 12.6,\ 14,\ 19,\ 22,\ 26.5,\ 34$ are in Fig. 10, and $K_c = 0.9633,\ 0.9764,\ 0.9821,\ 0.9885\ 0.9909,\ 0.9998 (K_c \to 1)$. For $\xi(t)$ exists, i.e., $\delta = 0.000001,\ 0.7,\ 3.5,\ 6$, the new trajectories and phase portraits about system (3.5)-(3.6) can be seen within Fig. 12, and $K_c = 0.9859,\ 0.9891,\ 0.9901,\ 0.9862\ (K_c \to 1)$. Accordingly, the homoclinic bifurcation and chaos in system (3.5)-(3.6) further demonstrated and tested through

the test value of K_c, Fig. 10 and Fig. 12.

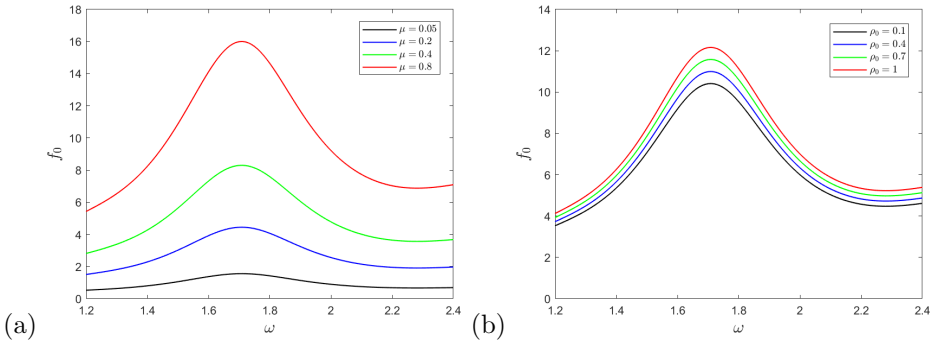


Fig. 5. The thresholds for homoclinic chaos in system (3.5)-(3.6) for (a): μ, (b): ρ_0 within (ω, f_0) plane when $\delta = 0$.

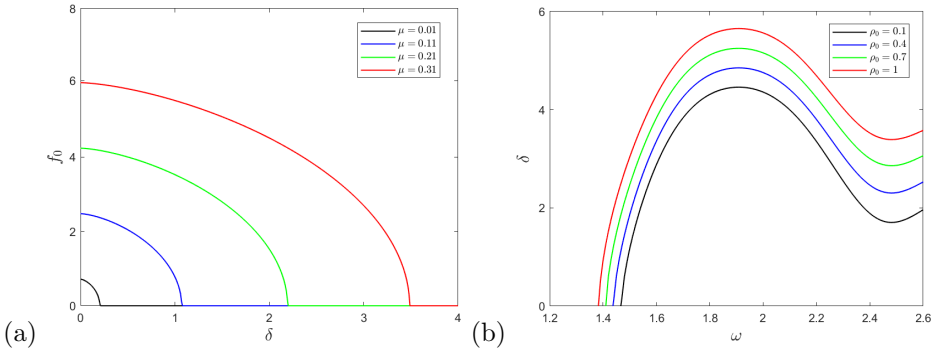


Fig. 6. The thresholds for homoclinic chaos in system (3.5)-(3.6) for (a): μ within plane (δ, f_0), (b): ρ_0 within plane (ω, δ).

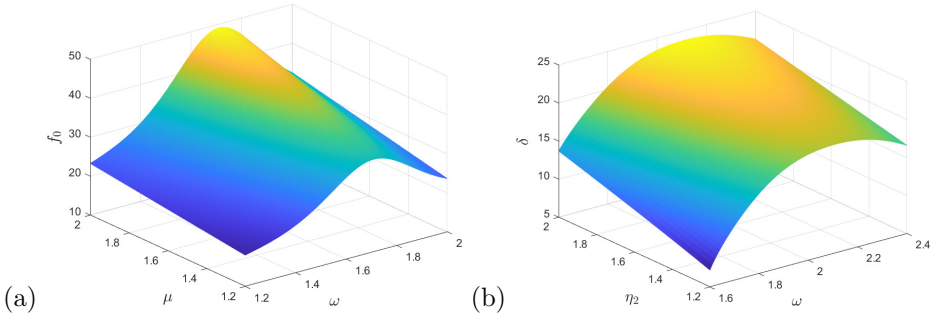


Fig. 7. The surface of homoclinic chaotic criticality in system (3.5)-(3.6) for (a): $\delta = 0$ within (ω, μ, f_0) space, (b): within (ω, η_2, δ) space.

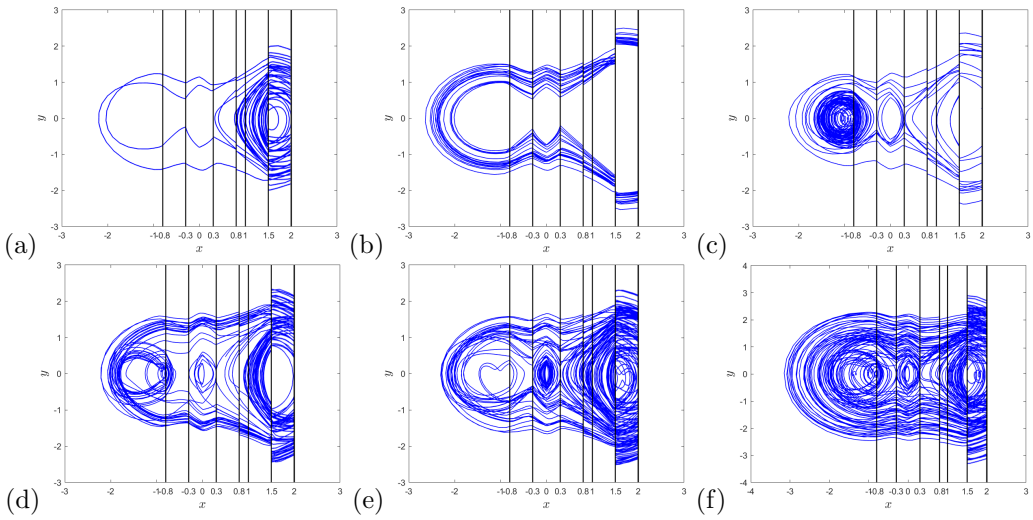


Fig. 8. The phase portraits in system (3.5)-(3.6) about (a): $f_0 = 12.6$, (b): $f_0 = 14$, (c): $f_0 = 19$, (d): $f_0 = 22$, (e): $f_0 = 26.5$, (f): $f_0 = 34$ when $\delta = 0$.

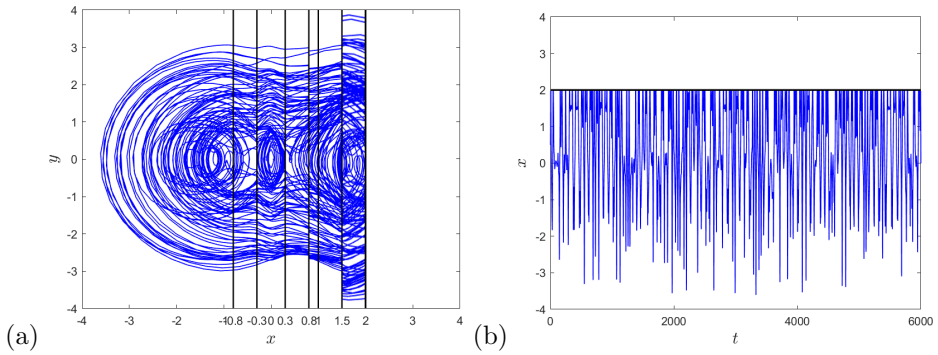


Fig. 9. The phase portrait and time serie in system (3.5)-(3.6) with $\delta = 0$ and $f_0 = 41$.

4 Conclusions

Our this work has developed the classical Melnikov theory. The Melnikov homoclinic chaotic theory has been extended to the general hybrid piecewise smooth systems subjected to elastic and rigid impacts under noise and impulsive excitation, then our corresponding Melnikov-type method is obtained. The corresponding Hamiltonian system, i.e., $\varepsilon = 0$, contains the quintuple well characteristic and homoclinic orbits with piecewise characteristics. The four switching manifolds, i.e., $x = \alpha_1, \alpha_2, \alpha_3, \alpha_4$, make $\mathbb{R}^2 = S_1 \cup \Sigma_1 \cup S_2 \cup \Sigma_2 \cup S_3 \cup \Sigma_3 \cup S_4 \cup \Sigma_4 \cup S_5$, and four subsystems correspond to S_1, S_2, S_3, S_4. The trajectories of the perturbed systems jump across Σ_1 by applying the reset mapping rule about the elastic impact, cross Σ_2 continuously, transversally jump across Σ_3 by impulsive excitation and then jump about the x-axis on Σ_4 symmetrically due to the rigid impact. But the trajectories won't cross Σ_4 in the existence of unilateral rigid constraint. Moreover, the corresponding Melnikov-type process and function are got, the conditions of homoclinic chaos in system (3.5)-(3.6) without and with the Gaussian white noise excitation are

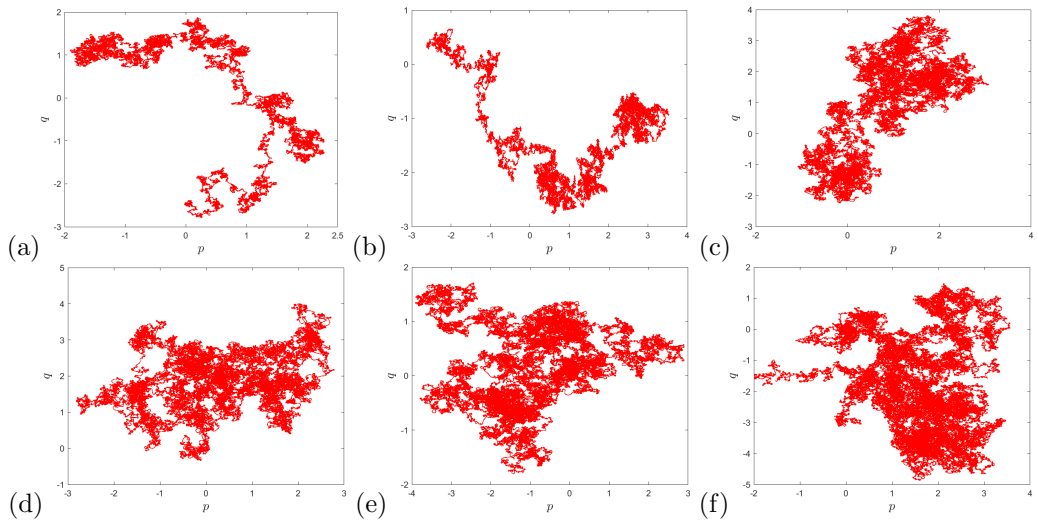


Fig. 10. The new phase portraits for system (3.5)-(3.6) within the newly established (p, q) about (a): $f_0 = 12.6$, (b): $f_0 = 14$, (c): $f_0 = 19$, (d): $f_0 = 22$, (e): $f_0 = 26.5$, (f): $f_0 = 34$ when $\delta = 0$.

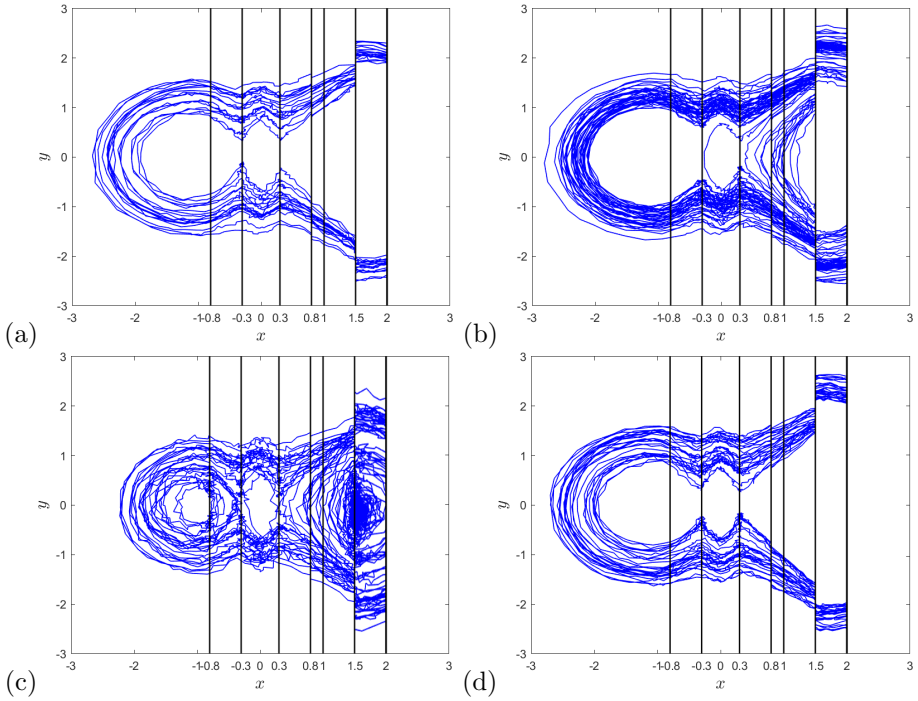


Fig. 11. The phase portraits for system (3.5)-(3.6) under $f_0 = 14$ and (a): $\delta = 0.000001$, (b): $\delta = 0.7$, (c): $\delta = 3.5$, (d): $\delta = 6$.

obtained.

In addition, the chaotic dynamics and homoclinic bifurcation in a concrete hybrid seven-piecewise feedback control system are analysed through our developed Melnikov method. All

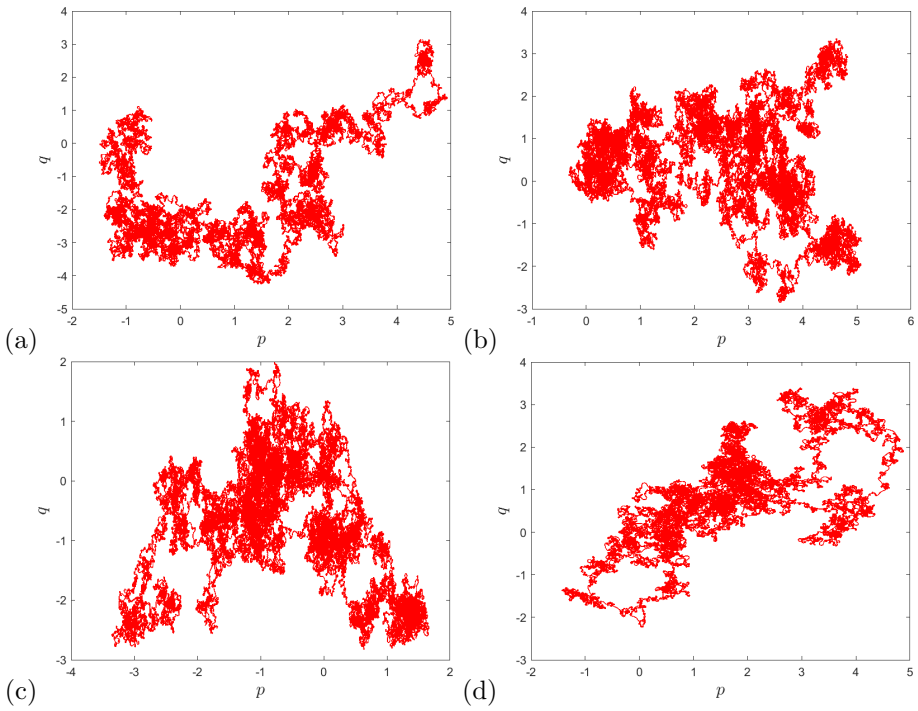


Fig. 12. The new phase portraits for system (3.5)-(3.6) within the newly established (p, q) under $f_0 = 14$ and (a): $\delta = 0.000001$, (b): $\delta = 0.7$, (c): $\delta = 3.5$, (d): $\delta = 6$.

analysis results and the correctness of method are demonstrated and tested through time series, phase portraits and 0-1 test method of chaos. Our these results and representative phenomena demonstrate that the transformation of noise excitation intensity δ can suppress and enhance chaotic degree in system (3.5)-(3.6). In the future work, we will further consider developing this Melnikov method into high-dimensional complicated piecewise systems.

Acknowledgements

This work was supported by the National Natural Science Foundation of China (NNSFC) (Nos. 12172340 and 12411530068), Shenzhen Natural Science Foundation, High-level Talent Introduction Plan of Guangzhou City, the Fundamental Research Funds for the Central Universities, China University of Geosciences (Wuhan) (Nos. G1323524005, and 2024XLB46), and the Young Top-notch Talent Cultivation Program of Hubei Province.

References

[1] P. Glendinning, M.R. Jeffrey, An introduction to piecewise smooth dynamics. Springer, Switzerland (2019).

[2] B. Brogliato, Nonsmooth impact mechanics. Spinger, London (1996).

[3] J.C. Ji, A.Y.T. Leung, Periodic and chaotic motions of a harmonically forced piecewise linear system. Int. J. Mech. Sci. 46 (2004), pp. 1807-1825.

[4] M.C. Mackey, L. Glass, Oscillation and chaos in physiological control systems. Science 197 (1977), pp. 287-289.

[5] J. Penalva, M. Desroches, A.E. Teruel, C. Vich, Dynamics of a piecewise-linear Morris–Lecar model: bifurcations and spike adding. J. Nonlinear Sci. 34 (2024) pp. 52.

[6] R. Cristiano, D.J. Tonon, M.Q. Velter, Hopf-Like bifurcations and asymptotic stability in a class of 3D piecewise linear systems with applications. J. Nonlinear Sci. 31 (2021), 65.

[7] V. Carmona, F. Fernández-Sánchez, D.D. Novaes, A succinct characterization of period annuli in planar piecewise linear differential systems with a straight line of nonsmoothness. J. Nonlinear Sci. 33 (2023), 88.

[8] M. Antali, P.L. Varkonyi, The nonsmooth dynamics of combined slip and spin motion under dry friction. J. Nonlinear Sci. 32 (2022), 58.

[9] K. Yagasaki, Nonintegrability of nearly integrable dynamical systems near resonant periodic orbits. J. Nonlinear Sci. 32 (2022), 43.

[10] Q.M. Xiang, Q.G. Yang, Chaos of multi-dimensional weakly hyperbolic equations with general nonlinear boundary conditions. J. Nonlinear Sci. 34 (2024), 59.

[11] J. Guckenheimer, P. Holmes, Nonlinear oscillations, dynamical systems and bifurcations of vector fields. Sprigner, New York (1997).

[12] S. Wiggins, Introduction to applied nonlinear dynamical systems and chaos. Sprigner, New York (2000).

[13] Y. Li, D.W. McLaughlin, Homoclinic orbits and chaos in discretized perturbed NLS systems: Part I. Homoclinic orbits. J. Nonlinear Sci. 7 (1997), pp. 211-269.

[14] X.D. Ma, Q.S. Bi, L.F. Wang, Complex periodic bursting structures in the Rayleigh–van der Pol–Duffing oscillator. J. Nonlinear Sci. 32 (2022), 25.

[15] J. Llibre, E. Perez-Chavela, Transversal homoclinic orbits in the collinear restricted three-body problem. J. Nonlinear Sci. 15 (2005), pp. 1-10.

[16] H. Li, J. Li, H.Z. Fei, G.Y. Hong, J.L. Dong, A.B. Yu, Chaotic dynamics of granules-beam coupled vibration: Route and threshold. Mech. Syst. Signal Process. 218 (2024), 111555.

[17] T. Sakajo, K. Yagasaki, Chaotic motion of the N-Vortex problem on a sphere: I. saddle-centers in two-degree-of-freedom Hamiltonians. J. Nonlinear Sci. 18 (2008), pp. 485-525.

[18] J.H. Zhang, W. Zhang, An extended high-dimensional Melnikov analysis for global and chaotic dynamics of a non-autonomous rectangular buckled thin plate. Sci. China Phys. Mech. Astron. 55 (2012), pp. 1679-1690.

[19] K. Yagasaki, Melnikov processes and chaos in randomly perturbed dynamical systems. Nonlinearity 31 (2018), pp. 3057-3085.

[20] M. Gidea, R. de la Llave, Global Melnikov theory in Hamiltonian systems with general time-dependent perturbations. J. Nonlinear Sci. 28 (2018), pp. 1657-1707.

[21] M. Kunze, Non-smooth dynamical systems. Springer, Berlin (2000).

[22] Z.D. Du, W.N. Zhang, Melnikov method for homoclinic bifurcations in nonlinear impact oscillators. Comput. Math. Appl. 50 (2005), pp. 445-458.

[23] S.B. Li, W. Zhang, Y.X. Hao, Melnikov-type method for a class of discontinuous planar systems and applications. Int. J. Bifurcat. Chaos 24 (2014), 1450022.

[24] F. Battelli, M. Fečkan, Nonsmooth homoclinic orbits, Melnikov functions and chaos in discontinuous systems. Phys. D 241 (2012), pp. 1962-1975.

[25] A. Granados, S.J. Hogan, T.M. Seara, The Melnikov method and subharmonic orbits in a piecewise-smooth system. SIAM J. Appl. Dyn. Syst. 11 (2012), pp. 801-830.

[26] S.B. Li, W.S. Ma, W. Zhang, Y.X. Hao, Melnikov method for a class of planar hybrid piecewise-smooth systems. Int. J. Bifurcat. Chaos 26 (2016), 1650030.

[27] S.B. Li, C. Shen, W. Zhang, Y.X. Hao, The Melnikov method of heteroclinic orbits for a class of planar hybrid piecewise-smooth systems and application. Nonlinear Dyn. 85 (2016), pp. 1091-1104.

[28] R.L. Tian, Y.F. Zhou, B.L. Zhang, X.W. Yang, Chaotic threshold for a class of impulsive differential system. Nonlinear Dyn. 83 (2016), pp. 2229-2240.

[29] R.L. Tian, Y.F. Zhou, Y.Z. Wang, W.J. Feng, X.W. Yang, Chaotic threshold for non-smooth system with multiple impulse effect. Nonlinear Dyn. 85 (2016), pp. 1849-1863.

[30] R.L. Tian, T. Wang, Y.F. Zhou, J. Li, S.T. Zhu, Heteroclinic chaotic threshold in a nonsmooth system with jump discontinuities. Int. J. Bifurcat. Chaos 30 (2020), 2050141.

[31] B.L. Zhou, Y.F. Jin, H.D. Xu, Subharmonic resonance and chaos for a class of vibration isolation system with two pairs of oblique springs. Appl. Math. Model. 108 (2022), pp. 427-444.

[32] S.B. Li, R. Xu, L.Y. Kong, Suppressing homoclinic chaos for a class of vibro-impact oscillators by non-harmonic periodic excitations. Nonlinear Dyn. 112 (2024), pp. 10845-10870.

[33] R.Y. Peng, Q.H. Li, W. Zhang, Chaos analysis of SD oscillator with two-frequency excitation. Nonlinear Dyn. 112 (2024), pp. 7649-7677.

[34] R.Y. Peng, Q.H. Li, W. Zhang, Homoclinic bifurcation analysis of a class of conveyor belt systems with dry friction and impact. Chaos Solit. Fract. 180 (2024), 114468

[35] S.G. Hu, L.Q. Zhou, Stochastic Hopf bifurcation and random chaos of the ship rolling dynamic system in random longitudinal wave induced by GWN. Ocean Eng. 286 (2023), 115572.

[36] Y.X. Li, Z.C. Wei, T. Kapitaniak, W. Zhang, Stochastic bifurcation and chaos analysis for a class of ships rolling motion under non-smooth perturbation and random excitation. Ocean Eng. 266 (2022), 112859.

[37] A.R. Bulsara, W.C. Schieve, E.W. Jacobs, Homoclinic chaos in systems perturbed by weak Langevin noise. Phys. Rev. A 41 (1990), pp. 668-681.

[38] M. Frey, E. Simiu, Noise-induced chaos and phase space flux. Physica D 63 (1993), pp. 321-340.

[39] H. Lin, S.C.S. Yim, Analysis of a nonlinear system exhibiting chaotic, noisy chaotic, and random behaviors. J. Appl. Mech. 63 (1996), pp. 509-516.

[40] Y.M. Lei, F. Zhang, X.Z. Shao, Chaos and chaos control of the Frenkel–Kontorova model with dichotomous noise. Int. J. Bifurcat. Chaos 27 (2017), 1750052.

[41] R.L. Tian, Z.J. Zhao, Y. Xu, Variable scale-convex-peak method for weak signal detection. Sci. China Tech. Sci. 64 (2021), pp. 331-340.

[42] N. Lu, Persistence of homoclinic orbits under white noise perturbation. SIAM J. Appl. Dyn. Syst. 15 (2016), pp. 1124-1142.

[43] D. Liu, Y. Xu, Random disordered periodical input induced chaos in discontinuous systems. Int. J. Bifurcat. Chaos 29 (2019), 1950002.

[44] Y.X. Li, Z.C. Wei, W. Zhang, M. Yi, Melnikov-type method for a class of hybrid piecewise-smooth systems with impulsive effect and noise excitation: Homoclinic orbits. Chaos 32 (2022), 073119.

[45] Z.C. Wei, Y.X. Li, I Moroz, W. Zhang, Melnikov-type method for a class of hybrid piecewise-smooth systems with impulsive effect and noise excitation: Heteroclinic orbits. Chaos 32 (2022), 103127.

[46] Y.X. Li, Z.C. Wei, W. Zhang, T. Kapitaniak, Melnikov-type method for chaos in a class of hybrid piecewise-smooth systems with impact and noise excitation under unilateral rigid constraint. Appl. Math. Model. 122 (2023), pp. 506-523.

[47] Q.J. Cao, M. Wiercigroch, E.E. Pavlovskaia, C. Grebogi, J.M.T. Thompson, Archetypal oscillator for smooth and discontinuous dynamics. Phys. Rev. E 74 (2006), 046218.

[48] Q.J. Cao, M. Wiercigroch, E.E. Pavlovskaia, C. Grebogi, J.M.T. Thompson, Piecewise linear approach to an archetypal oscillator for smooth and discontinuous dynamics. Phil. Trans. R. Soc. A 366 (2008), pp. 635-652.

[49] Y.W. Han, Q.J. Cao, Y.S. Chen, M. Wiercigroch, Chaotic thresholds for the piecewise linear discontinuous system with multiple well potentials. Int. J. Nonlin. Mech. 70 (2015), pp. 145-152.

[50] B.L. Zhou, Y.f. Jin, H.D. Xu, Global dynamics for a class of tristable system with negative stiffness. Chaos Solit. Fract. 162 (2022), 112509.

[51] X.Y. Huang, Q.J. Cao, S. Lenci, The complicated behaviours of a novel model of smooth and discontinuous dynamics with quasi-zero-stiffness property. Nonlinear Dyn. (2024) 112, pp. 20879-20902.

[52] Y.F. Zhang, H.D. Xu, J.W. Zhang, Global dynamics for impacting cantilever beam supported by oblique springs. Chaos Solit. Fract. 169 (2023), 113179.

[53] S.B. Li, C. Shen, W. Zhang, Y.X. Hao, Homoclinic bifurcations and chaotic dynamics for a piecewise linear system under a periodic excitation and a viscous damping. Nonlinear Dyn. 79 (2015), pp. 2395-2406.

[54] X.L. Yang, Y. Xu, Z.K. Sun, Effect of Gaussian white noise on the dynamical behaviors of an extended Duffing-van der Pol oscillator. Int. J. Bifurcat. Chaos 16 (2006), pp. 2587-2600.

[55] K.H. Sun, X. Liu, C.X. Zhu, The 0–1 test algorithm for chaos and its applications. Chin. Phys. B 19 (2010), 110510.

[56] L.G. Yuan, Q.G. Yang, C.B. Zeng, Chaos detection and parameter identification in fractional-order chaotic systems with delay. Nonlinear Dyn. 73 (2013), pp. 439-448.